PolyPublie
Polytechnique Montréal

POLYTECHNIQUE MONTRÉAL
UNIVERSITÉ D'INGÉNIERIE

Titre: Title:	Easy to build, modular and large scale pipe conveying fluid experimental setup
Auteurs: Authors:	Morgan Demenois, Hongyan Miao, & Frederick Gosselin
Date:	2023
Type:	Article de revue / Article
Référence: Citation:	Demenois, M., Miao, H., & Gosselin, F. (2023). Easy to build, modular and large scale pipe conveying fluid experimental setup. HardwareX, 15, e00460 (30 pages). https://doi.org/10.1016/j.ohx.2023.e00460

Document en libre accès dans PolyPublie
Open Access document in PolyPublie

URL de PolyPublie: PolyPublie URL:	https://publications.polymtl.ca/56343/
Version:	Version officielle de l'éditeur / Published version Révisé par les pairs / Refereed
Conditions d'utilisation: Terms of Use:	Creative Commons Attribution-Utilisation non commerciale-Pas d'oeuvre dérivée 4.0 International / Creative Commons Attribution-NonCommercial-NoDerivatives 4.0 International (CC BY-NC-ND)

Document publié chez l'éditeur officiel
Document issued by the official publisher

Titre de la revue: Journal Title:	HardwareX (vol. 15)
Maison d'édition: Publisher:	Elsevier
URL officiel: Official URL:	https://doi.org/10.1016/j.ohx.2023.e00460
Mention légale: Legal notice:	

Ce fichier a été téléchargé à partir de PolyPublie, le dépôt institutionnel de Polytechnique Montréal
This file has been downloaded from PolyPublie, the institutional repository of Polytechnique Montréal

https://publications.polymtl.ca

HardwareX 15 (2023) e00460

Contents lists available at ScienceDirect

HardwareX

journal homepage: www.elsevier.com/locate/ohx

Hardware article

Easy to build, modular and large scale pipe conveying fluid experimental setup

Morgan Demenois, Hong Yan Miao, Frédérick P. Gosselin *

Department of Mechanical Engineering, Polytechnique Montréal, Canada

ARTICLE INFO

Keywords:
Fluid–structure interactions
Experimental study
Vibrations
Non-linear dynamics
Stability
Easy-to-build

ABSTRACT

The pipe conveying fluid is a classic fluid structure interaction experiment. First studied for industrial applications such as liners and pipelines, it became a ‘‘paradigm" of non-linear dynamics in the same way as the vertical rotating shaft. Hundreds of papers studying different pipe instabilities and different phenomena with various numerical and analytical methods have been published in the last decades. However, many studies lack the comparison with experimental data to validate the analytical models and numerical simulations. Indeed, designing and building a pipe conveying fluid experimental setup can prove to be a long and a burdensome process. This paper presents an easy to build pipe conveying fluid experimental setup built in the LM2 laboratory at Polytechnique Montréal. Fig. 1 presents the global architecture of this experimental rig. This large scale setup uses relatively high speed cameras to track the pipe in three dimensions. It does not require heavy construction or major plumbing and electrical work. Moreover, it is removable and can be modified easily to observe different phenomena with various large scale pipes or boundary conditions. Lastly, it is relatively inexpensive as it costs less than 20 000 US dollars including all the sensors and acquisition systems.

Specifications table	
Hardware name	Pipe conveying fluid experimental setup
Subject area	Engineering and material science
Hardware type	Mechanical engineering and materials science
Closest commercial analog	No commercial analog is available.
Open source license	CERN Open Hardware License (OHL)
Cost of hardware	Approximately 20 000 US dollars
Source file repository	https://doi.org/10.17632/xtwrf8859b.3

1. Hardware in context

The pipe conveying fluid experiment is a conceptually simple fluid–structure interaction problem: a garden hose comes to life and wiggles upon being subjected to a high enough flowrate. Many variants of the pipe conveying fluid exist and have been thoroughly studied both analytically and numerically [1]. The pipe can be either vertical or horizontal and can be maintained using different types of boundary conditions. It is a system of great interest to researchers for two main reasons. Firstly, the pipe conveying fluid models many physical and industrial systems such as pipelines or oil rigs liners and hangers [2]. Secondly, it is a model experiment

* Corresponding author.
E-mail addresses: hong-yan.miao@polymtl.ca (H.Y. Miao), frederick.gosselin@polymtl.ca (F.P. Gosselin).

https://doi.org/10.1016/j.ohx.2023.e00460
Received 23 March 2023; Received in revised form 26 June 2023; Accepted 26 July 2023
Available online 9 August 2023
2468-0672/© 2023 The Author(s). Published by Elsevier Ltd. This is an open access article under the CC BY-NC-ND license (http://creativecommons.org/licenses/by-nc-nd/4.0/).

well suited to test and develop new numerical methods to solve non-linear dynamics problems [3,4]. Indeed, it is a simple and inexpensive system to build in a university laboratory. However, despite its apparent hardware simplicity, the pipe conveying fluid is an incredibly complex system that displays rich dynamics phenomena ranging from linear planar dynamic to heavily non-linear and even chaotic three dimensional behaviour. Despite the great scientific knowledge that can be acquired through the study of the pipe conveying fluid, few experimental studies are conducted to assist numerical studies and even fewer studies present detailed experimental setup construction. A vertical pipe conveying fluid experimental setup was adapted for various studies by Paidoussis and is presented in many studies [5,6]. Other examples of pipe conveying fluid setups are presented for long pipes [7] or for pipes subjected to transverse excitation [8,9].

The setup presented in this article is suited to study a vertical pipe conveying fluid with a clamped top end. In this special case, the second end is free but can be easily modified to a clamped tip or springs for example to study the dramatically different behaviour of the clamped–clamped pipe or the effect of springs. This setup, due to its assembly and operation simplicity, is being used at Polytechnique Montréal to develop new numerical methods combining experimental data from the pipe conveying fluid experiment with physics based modelling. The main advantage of the experimental setup we propose compared to existing ones is the data acquisition system. Indeed, the cameras allow us to capture the entire shape of the pipe at every frame in a contactless way. We do not have to constrain the motion of the pipe to a planar motion to capture it and we do not have to put anything influencing the pipe motion on the pipe. The other advantage of this setup is its flexibility and its simple assembly. Thanks to the aluminium extrusion we can assemble and modify easily the setup to change the boundary conditions of the pipe for example.

This setup is still relevant even if it is now possible to model the pipe behaviour with semi-analytical and numerical models. Indeed, the advantage of this setup compared to theoretical models is that it allows us to study the actual pipe conveying fluid with its defects and phenomena that cannot be modelled in a classic simulation. The intent of this setup was to use it as a test bench to learn methods to perform state or parameter estimation to build a digital twin of a physical system with artificial intelligence. This setup allows us to capture available data with its defects and noise similarly to real industrial application. Hence, with this setup we learn to build a more robust digital twin that can work with imperfect and incomplete data.

2. Hardware description

The architecture of the pipe conveying fluid setup is inspired by Paidoussis [5] and shown in Fig. 2 with the principal components labelled. The water from the pipe flow goes to the main 35 USG plastic tank (1) through a drain in the transparent tank before going back in the pump. A two Horse Power (HP) centrifugal pump (2) generates the flow in the circuit. The pump is powered by a tri-phase variator drive to control the flowrate. The drive controls the current output frequency from 0 to 60 Hz with a 0.1 Hz frequency step. A flow control valve after the pump controls the flowrate more precisely if needed. The water then goes into an accumulator 15 USG steel tank (3) rated for a pressure up to 75 psi. In this accumulator tank, the free liquid surface between the water and the air on the top mitigates the potential fluctuations in the flow induced by the pump. The flexible plastic tubing in the circuit also adds damping to the system and makes the assembly of the setup easier. A magnetic flowmeter (8711, Rosemount) with a 3/4" flowtube and a transmitter (8732, Rosemount) (4) measure the volumic flowrate in the circuit. The flow velocity is read directly on the flowmeter or is stored in a text file with a current acquisition card (NI9203, National Instrument). The flowmeter delivers a 4–20 mA current signal that is scaled to the needed flowrate range. The section of the circuit then increases to a 2 inches diameter from a 3/4 inch diameter. A flow straightener (5) built with plastic straws taped together is fixed in the higher diameter section. This flow straightener with low diameters straws breaks large movements in the flow and also helps to get a laminar flow. After the flow straightener, the diameter of the circuit shrinks back to 3/4 inch to improve the flow quality. At the end of the circuit, the ‘‘pipe conveying fluid’’ is fixed with a clamp and a hose fitting on which the pipe is embedded. The origin point of the pipe is considered to be the point where the hose fitting in the pipe ends. The pipe is then contained in a $4 \times 4 \times 2$ ft acrylic and transparent tank (6) supported by an aluminium extrusion structure (7). The water then flows back to the main tank mentioned before. A white plastic liner covers up the tank and contain the splashes. Two relatively high speed cameras (BFS-U3-20S4C-C, FLIR) with two lenses (8 mm FL-CC0814-2M, Ricoh) (8) and (8’) are fixed with T-slotted rails. These fixations allow the operator to move the cameras in both directions. The lenses are as close as possible to the plastic plates of the tank to focus beyond the water droplets on the tank. A water repellent spray applied on the tank walls increases the dripping of the water. The two sides of the tank opposite to the cameras are covered with white opaque plastic sheets to have a white uniform background for the cameras and to facilitate image treatment.

The pipe used for the pipe conveying fluid setup is cast in the laboratory with a mould inspired by Ref. [10] and shown in Fig. 3. The mould is made of two aluminium parts (2) and (3) that were machined with a three axis milling machine. Four dowel pins and 14 screws hold these two parts aligned and maintained together. Two 3D printed cap (6) and (6’) close each side of the mould. A white plastic washer is fitted in these caps to centre a stainless steel rod (4) in the mould creating the lumen of the pipe. Four threaded rods (5) fix the 3D printed caps at each ends of the aluminium mould. The mould is held vertical on a plank and the rubber-silicon is injected on the bottom cap to obtain the pipe conveying fluid (1).

How this new hardware could help the reader:

- Capture the three dimensional position of the whole pipe.
- Allows to study different kind of pipes with different boundary conditions.
- Generate training or validation data for classical or machine learning numerical simulations.
- Retrieve live data from the pipe behaviour.

Table 1
Design files summary.

Design filename	File type	Open source license	Location of the file
MouldTopAlu.stp	CAD file	**CERN Open Hardware License (OHL)**	MouldTopAlu.stp
MouldBotAlu.stp	CAD file	**CERN Open Hardware License (OHL)**	MouldBotAlu.stp
MouldCapPLA.stp	CAD file	**CERN Open Hardware License (OHL)**	MouldCapPLA.stp
CameraFixTop.stp	CAD file	**CERN Open Hardware License (OHL)**	CameraFixTop.stp
CameraFixBot.stp	CAD file	**CERN Open Hardware License (OHL)**	CameraFixBot.stp
PipeFixTop.stp	CAD file	**CERN Open Hardware License (OHL)**	PipeFixTop.stp
PipeFixBot.stp	CAD file	**CERN Open Hardware License (OHL)**	PipeFixBot.stp
MouldCapPLA.stl	CAD file	**CERN Open Hardware License (OHL)**	MouldCapPLA.stl
CameraFixTop.stl	CAD file	**CERN Open Hardware License (OHL)**	CameraFixTop.stl
CameraFixBot.stl	CAD file	**CERN Open Hardware License (OHL)**	CameraFixBot.stl
PipeFixTop.stl	CAD file	**CERN Open Hardware License (OHL)**	PipeFixTop.stl
PipeFixBot.stl	CAD file	**CERN Open Hardware License (OHL)**	PipeFixBot.stl

3. Design files summary

The design files are available at [11] for the parts of the setup that were not commercially available and therefore were 3D printed or machined. The 3D printed parts were built out of Polylactic Acide (PLA) with a 3D printer (3, Ultimaker) and the STL files used for printing are provided along 3D models in STEP formats. The machined parts are made of aluminium and were milled with a three axis milling machine. Only the 3D models in STEP formats are provided since the G-codes files used for machining are specific to the milling machine used for the operation (see Table 1).

- MouldTopAlu.stp: One of the two main parts (3) used to mould the pipe. It is made of an aluminium block milled with a three axis milling machine. This part is assembled with the bottom part of the mould.
- MouldBotAlu.stp: The second main part (2) used to mould the pipe. It is also made of aluminium with a three axis milling machine. Threaded holes were machine in this part to allow tightening with the top part of the mould.
- MouldCapPLA.stp: This part (6) has to be 3D printed in PLA twice to complete the mould. It goes at each end of the mould to close it.
- CameraFixTop.stp: This part is 3D printed in PLA. It goes on top of the acrylic tank walls of the setup to maintain the rail on which the cameras are clamped.
- CameraFixBot.stp: This part is 3D printed in PLA. It goes at the bottom of the acrylic tank and is clamped on the edge. It maintains the rail on which the cameras are fixed.
- PipeFixTop.stp: This part is 3D printed in PLA and four threaded inserts are inserted in the side holes. These threaded inserts are used to fix this part on the aluminium extrusions structure. This part is used to fix the top of the flow-straightener before the fixation of the pipe conveying fluid.
- PipeFixBot.stp: This part is 3D printed in PLA and four threaded inserts are inserted in the side holes. These threaded inserts are used to fix this part on the aluminium extrusions structure. This part is used to fix barbed fitting on which the pipe conveying fluid is fitted.

4. Bill of materials summary

This section presents the parts and materials bought to build this experimental setup. The models and sources of each parts shown in Table 2 are a suggestion and other options exist. The flowmeter, the centrifugal pump and the sensors acquisition cards were recovered from previous applications in the laboratory. Wall and ground fixations are not provided and have to be chosen according to the laboratory walls and floor characteristics. Only the main parts are presented in this bill of materials and is available in the repository in csv format (Bill of material).

The motor and the pump are not commercially available anymore. We recommend a 2HP centrifugal pump. An adequate recommendation is the FAC200-2HP-575V with a speed variator 2HP-575V VACCON. This pump, motor and variator is adequate for the electrical installation that we have in our lab, i.e. tri-phase 575 V. We recommend readers to check the power source available in their lab and to consult an electrician and a water pump specialist to chose an appropriate pump for their labs. We do not provide a diagram of the electrical connections since an electrician did the electric installations and we recommend readers to consult an electrician for their electric installation as well.

5. Build instructions

Fig. 1 shows a complete 3D representation of the experimental setup and Fig. 2 shows the actual setup installed in the laboratory. On these representations of the setup, we can identify 8 sub-assemblies:

- Main tank (1)
- Pump (2)

Table 2
Bill of materials summary.

Designator	Component	Number	Cost per unit - USD	Total cost - USD	Source of materials	Material type
Rosemount 8711TSA010T1N0 flowmeter	Magnetic flowmeter	1	2200	2200	See local Rosemount provider	Non-specific
Rosemount 8732CT12N0M4 transmitter	Integral transmitter mounted on the flowtube	1	2800	2800	See local Rosemount provider	Non-specific
Secondary tank 3669K27	Pressure rated tank used to attenuate fluctuation in the flow after the pump	1	381.4	381.4	Part link	Metal
Heavy shelf brackets 2736A723	Brackets used to support the tank on the wall	2	18.84	37.68	Part link	Metal
Clamp https 3116T75	Clamp used to maintain the tank to the wall	1	234.26	234.26	Part link	Metal
Baldor M3559 motor	Motor used for the pump	1	Not commercially available	Not commercially available	Part link	Non-specific
Price Pump Model OH75	Centrifugal pump mounted on the motor	1	Not commercially available	Not commercially available	Part link	Non-specific
Siemens Sinamics V20 drive	Electrical drive controlling the motor	1	380	380	See local Siemens provider	Non-specific
Main plastic tank 3764K31	Plastic tank used to store the circuit water	1	690	690	Part link	Polymer
Wall acrylic sheets 8560K435	Translucid side plates of the tank	4	105.64	422.56	Part link	Polymer
Bottom acrylic sheet 8560K272	Bottom plate of the tank	1	354.97	354.97	Part link	Polymer
Aluminium T-slotted extrusion 47065T102-47065T602	T-slotted extrusions for the acrylic tank support	14	27.58	386.12	Part link	Metal
BFS-U3-20S4C-C Camera	USB3 Cameras	2	825	1650	See local camera supplier	Non-specific
FL-CC0814-2M Lens	6mm Lenses	2	135	270	See local camera supplier	Non-specific
Aluminium T-slotted extrusion 47065T704	T-slotted extrusions for the pipe conveying fluid support	6	40.77	244.62	Part link	Metal
NI 9203	Current acquisition card	1	900	900	See local NI supplier	Non-specific
NI 9263	Voltage acquisition card	1	750	750	See local NI supplier	Non-specific
NI cDAQ 9174	Acquisition cards chassis	1	1420	1420	See local NI supplier	Non-specific
NI 9977	Blank fill cards	2	60	120	See local NI supplier	Non-specific
OOMOO30 rubber-silicon	Rubber-silicon kit used for the pipe conveying fluid	1	45	45	Part link	Polymer
Aluminium bars 8975K253-8975K998	Aluminium used to machine MouldTopAlu and MouldBotAlu	2	75.09	150.18	Part link	Metal

- Accumulator tank (3)
- Flowmeter (4)
- Flow-straightener and pipe fixation (5)
- Acrylic tank (6)
- Acrylic tank support (7)
- Cameras (8)

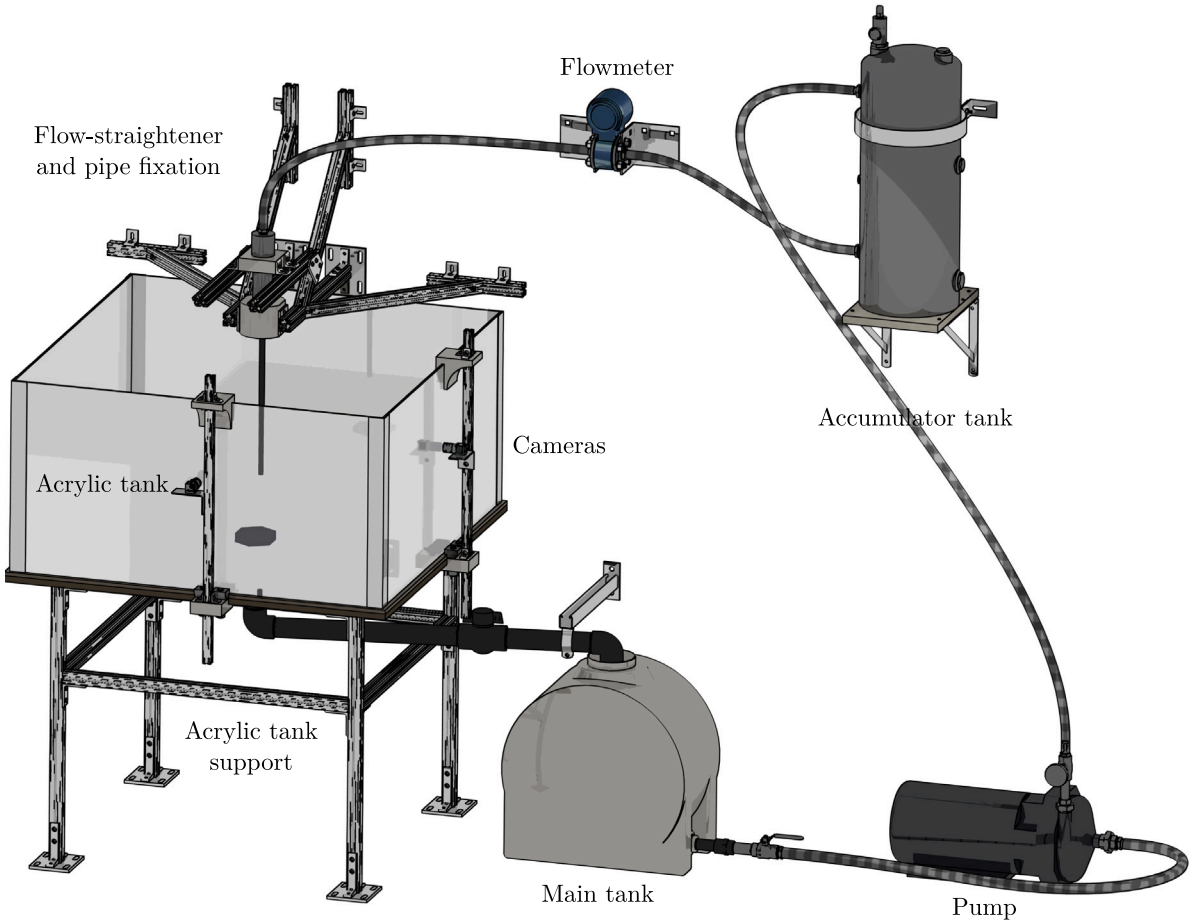

Fig. 1. 3D representation of the whole setup.

In addition to these 8 sub-assemblies, we add the mould used to cast the pipe conveying fluid. We provide instructions on how to assemble these 9 sub-assemblies in the following sections.

5.1. Main tank

This section presents how the main plastic tank storing the circuit water is connected to the acrylic tank and to the pump. Fig. 4 shows a 3D representation of this sub-assembly and Fig. 5 shows how to assemble this group:

- Screw the 2" vertical PVC pipe on the drain of the acrylic tank with thread sealant tape.
- Screw the first PVC elbow, the first PVC pipe, the PVC valve the second PVC pipe and the second PVC elbow using thread sealant tape.
- Adjust the pipes to align the bottom of the second PVC elbow with the top of the main tank.
- Fit the hanging clamp around the PVC pipe and fix it to the wall with the wall fixation.
- On the output drain of the main tank, screw the PVC pipe, the PVC to stainless pipe adapter, the stainless pipe, the stainless valve and the barbed fitting with thread sealant tape.

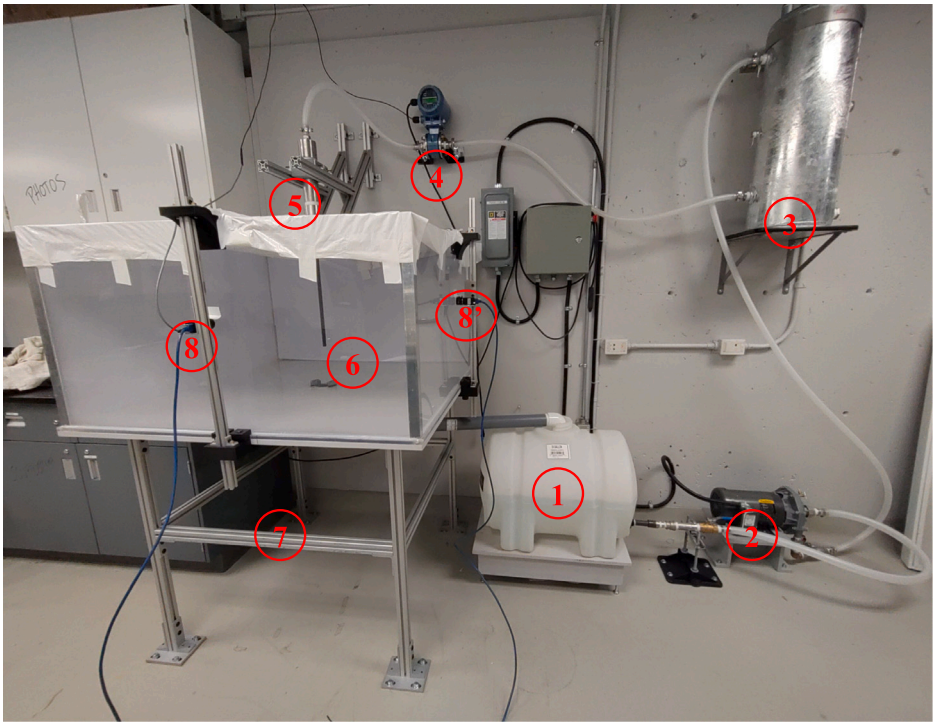

Fig. 2. Photo of the experimental setup with important parts circled in red.

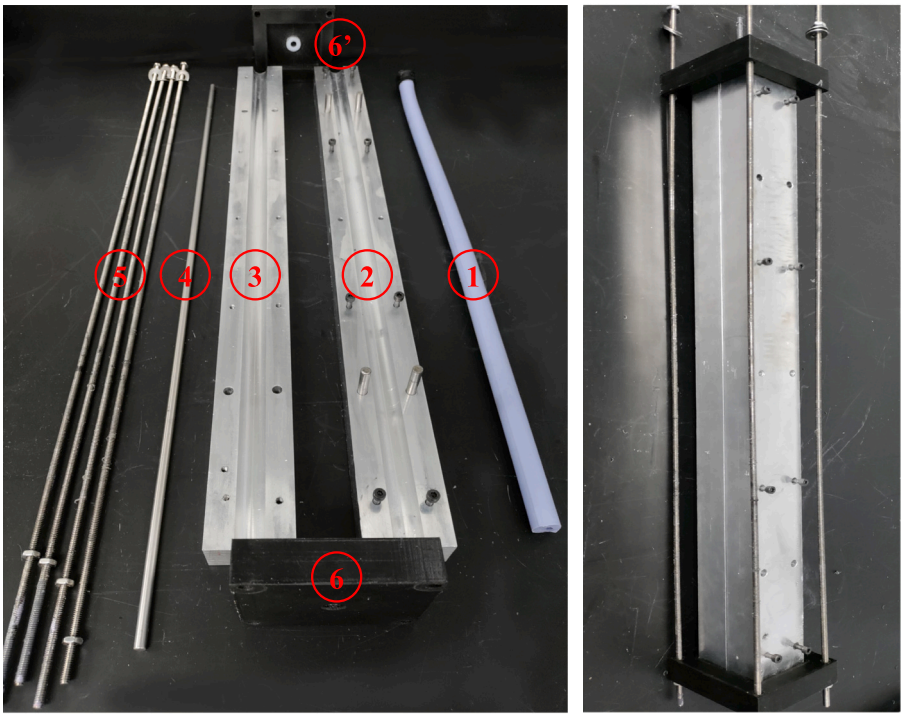

Fig. 3. Photo of the mould used to cast the pipe conveying fluid with rubber silicon.

Fig. 4. 3D representation of the main tank and of its connection to the acrylic tank and to the pump.

5.2. Pump

Here we present the pump sub-assembly with its input and output tubing. Fig. 6 shows a 3D representation of the pump assembly and Fig. 7 shows an exploded view of the assembly. The instruction to build this assembly are:

- Fix the pump on the floor of the lab.
- Fit the threaded part of both unions on the output and input of the pump with thread sealant tape.
- Fit the other part of the input union to the barbed fitting connecting the pump to the main tank with a flexible hose.
- Fit the other part of the output union to the stainless pipe, the flow control valve and the barbed fitting connecting the pump to the secondary tank with a flexible hose.

5.3. Accumulator tank

This section presents the assembly procedure to build the accumulator tank assembly. Fig. 8 shows a 3D representation of this sub-assembly while 9 presents an exploded view. Assemble the secondary tank as follows:

- Fix the two heavy duty shelf brackets on the wall.
- Fix the wood plank on the brackets with the screws and nuts.
- Put the secondary tank on the wood plank.
- Fix the clamped to the wall to maintain the top of the tank.
- Fit the pressure relieve valve on the top hole with thread sealant tape.
- Fit the two barbed fitting on the two 1" side holes with thread sealant tape to connect the tank to the pump and to the flowmeter with flexible hoses.
- Close the rest of the holes with the caps and with thread sealant tape.

5.4. Flowmeter

This section explains how to assemble the flowmeter in the circuit. Fig. 10 shows a 3D model of the flowmeter assembly and Fig. 11 presents an exploded view of the parts of this assembly. The reader shall follow the subsequent steps to build this sub-assembly:

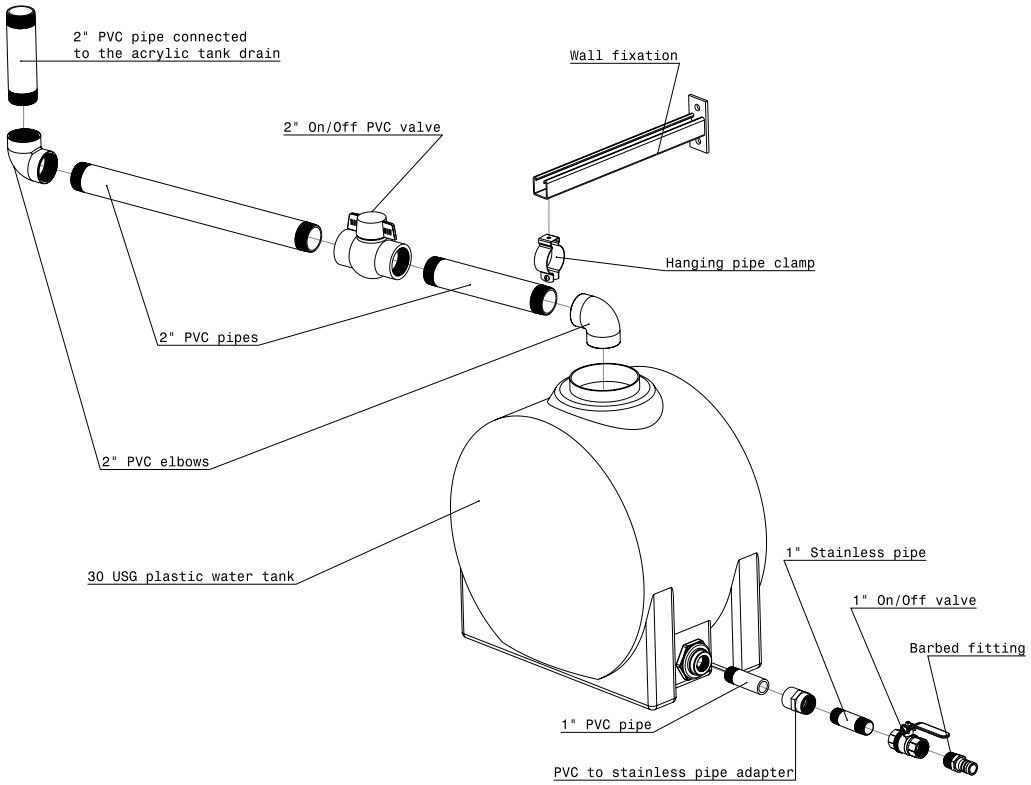

Fig. 5. Exploded view representing the assembly of the main tank with its tubing.

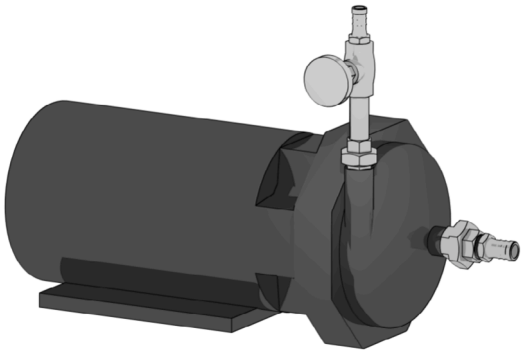

Fig. 6. 3D representation of the pump and of its tubing.

- Fit the four threaded rods in the four holes of the flowmeter.
- On each side of the flowtube, approach the rubber gaskets and fit them on the four threaded rods.
- On each side of the flowtube,approach the flanges and fit them on the four threaded rods.
- On each side of the flowtube, approach the steel brackets an fit them on the two backside threaded rods.
- Tighten the gaskets, flanges and brackets on the flowtube with the washers and nuts on the four threaded rods.
- Fix the steel brackets to the wall to fix the whole assembly to the wall.
- Fit the two barbed fitting on the two flanges with thread sealant tape.

5.5. Flow-straightener and pipe fixation

This section treats the fixation of the flow-straightener and the clamping of the top of the pipe conveying fluid. This structure has to be as rigid as possible to provide a perfect steady boundary condition for the pipe even when the flowrate is high and when the pipe is vibrating heavily. Fig. 12 presents a 3D view of this assembly while Fig. 13 shows an exploded view of its components.

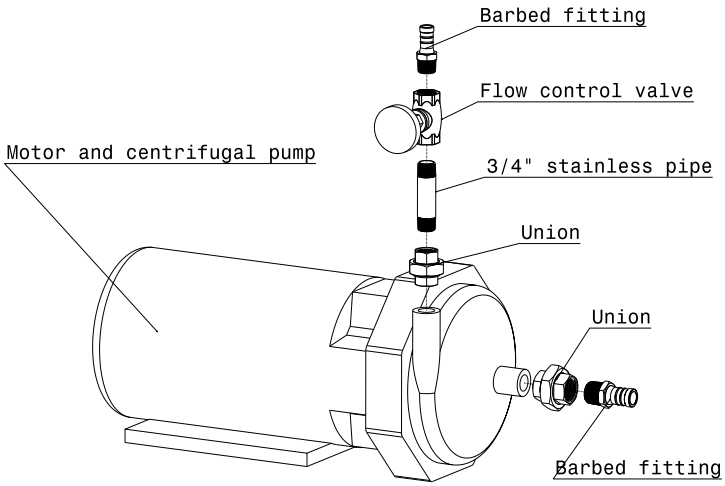

Fig. 7. Exploded view representing the assembly of the pump with its tubing.

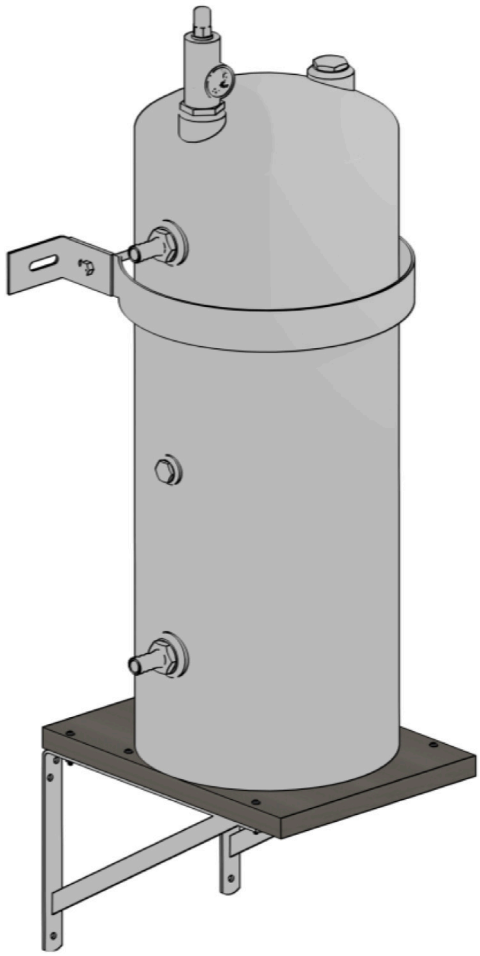

Fig. 8. 3D representation of the accumulator tank.

For readability purpose, the exploded view presents only half of the structure and the screws and nuts are not presented. Follow these step to assemble the structure:

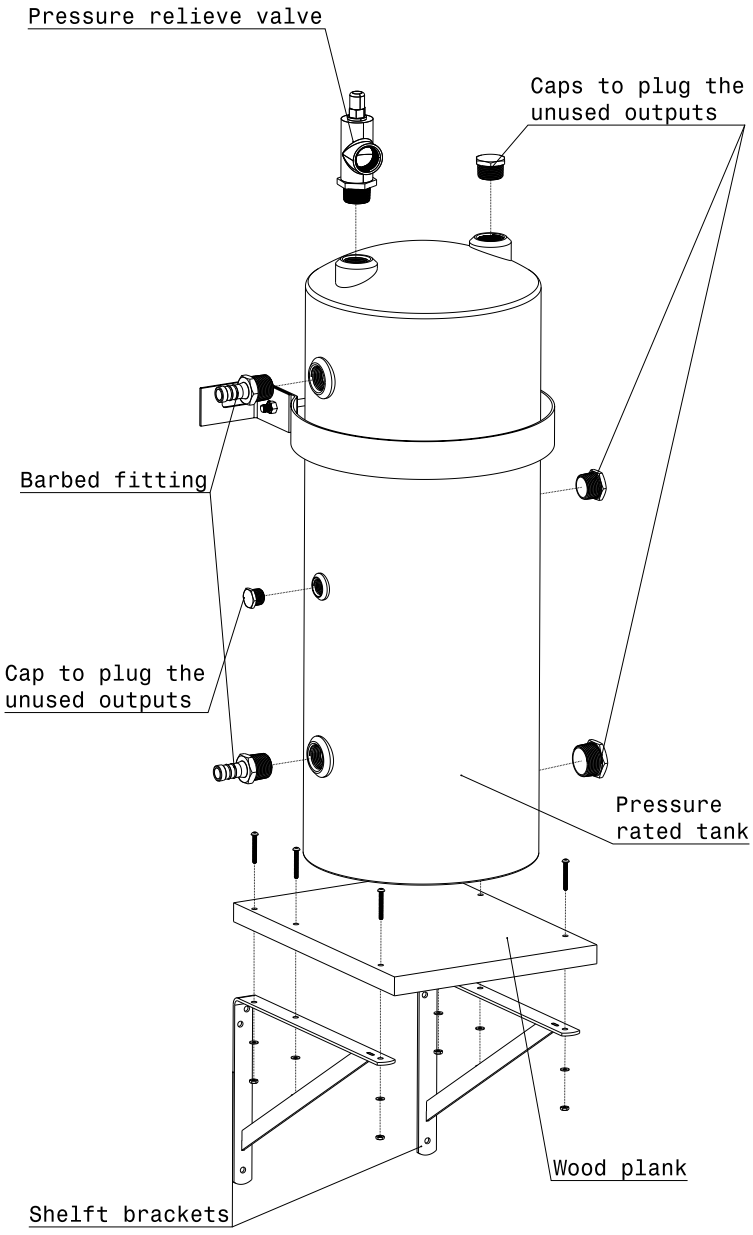

Fig. 9. Exploded view representing the assembly of the accumulator tank.

- Fit the 2" pipe from the flow-straightener in the PipeTopFix 3D printed part.
- Screw both stainless reducer on both sides of the pipe with thread sealant tape.
- Screw the two barbed fitting on the two reducers with pipe sealant tape.
- Fit the pipe conveying fluid on the bottom barbed fitting and clamp it with a worm drive.
- Fit the PipeFixBot 3D printed part on the bottom stainless reducer.
- Assemble the two T-slotted extrusions structures (only one is represented on the exploded view).
- Fix the two T-slotted extrusions structures on the two 3D printed parts with the mounting plate and the corner fixations.
- Fix the whole assembly on the wall.

5.6. Acrylic tank

This sections describes how to assemble the acrylic tank. This tank is used to contain the water coming from the pipe conveying fluid. It is large enough not to hinder the pipe movement and transparent to allow the observation of the pipe. Fig. 14 shows a 3D

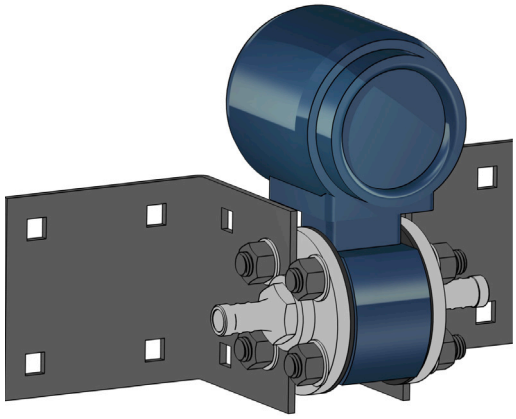

Fig. 10. 3D representation of the flowmeter and of its tubing.

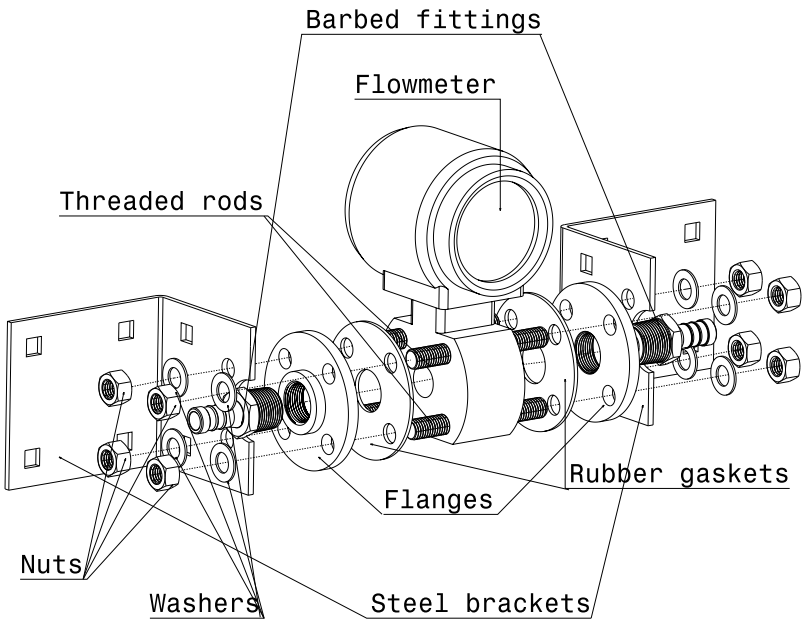

Fig. 11. Exploded view representing the assembly of the flowmeter with its tubing.

model of the acrylic tank. It is built with four side acrylic sheets of a quarter inch thickness and with a thicker half inch acrylic plate for the bottom. Aluminium corners are glued at each corner and a wood plank is glued to the bottom sheet to improve the rigidity. A plastic drain is fitted at the middle of the bottom planks.

Fig. 15 presents the assembly of the tank following the subsequent steps:

- Glue the bottom acrylic sheet on a wood plank of the same width to increase the rigidity of the tank.
- Drill a hole in both the wood plank and the bottom acrylic sheet to fit the drain.
- Fit the drain in the hole with the rubber gasket.
- Carve a groove of the width of the side acrylic walls in the bottom acrylic sheet.
- Put the acrylic walls in the groove and use silicon to glue the acrylic sheets together.
- Glue the aluminium corners at each corners to improve the rigidity and minimize the leaks.
- Stick white plastic sheets to two walls of the tank to obtain plain white backgrounds for the cameras.

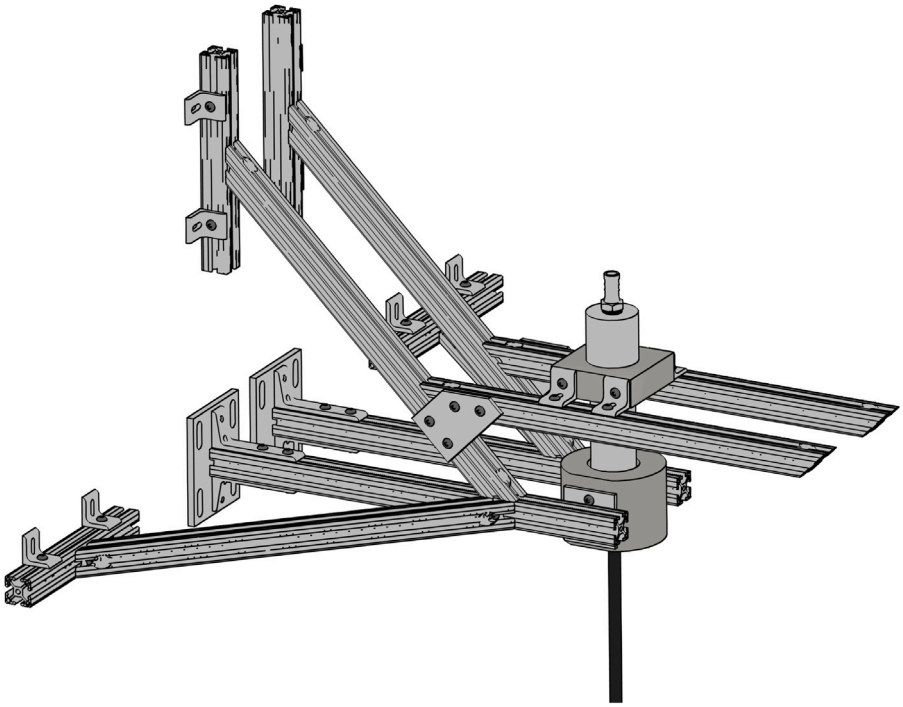

Fig. 12. 3D representation of the structure supporting the flow-straightener and the pipe conveying fluid clamping.

5.7. Acrylic tank support

This sections describes how to assemble the support of the acrylic tank. This support is built with T-slotted aluminium extrusions which are lightweight, easy to assemble and offer a great use flexibility. Fig. 16 presents a 3D representation of this sub-assembly.

This assembly is composed of 14 extrusions held together with corner brackets. The fixation of one bracket on one extrusion is highlighted in Fig. 17. The procedure is as follows:

- Insert the four sliding nuts in the T-slotted extrusions. Position the nuts as closely as possible to their final positions.
- Position the corner fixations on one of the T-slotted extrusions, align the nuts with the holes of the corner and engage the screws.
- Repeat the precedent operation with the second T-slotted extrusion.
- Tighten the four screws one after the other while adjusting the nuts positions in the extrusions.

Fig. 18 shows how to assemble the support of the acrylic tank. To improve readability one of the corner of the support is missing from the exploded view as well as the screws and nuts. It is important to follow a certain assembly order to make sure that we can slide the nuts into the T-Slotted extrusions. To assemble the support the reader shall follow these steps:

- Fix four T-Slotted extrusions on the floor mountings to build the “legs” of the support
- Fix the T-Slotted extrusions called “Bottom reinforcements” on the legs. It is important to fix these before the one called “Horizontal” to be able to slide the nuts in the T-Slotted extrusions.
- Fix the T-slotted extrusions called “Top reinforcements” on the ones called “Horizontal”
- Fix the “Horizontal” T-slotted extrusions (previously fixed to the “top reinforcements”) on the “legs”

5.8. Cameras

This section explains how the USB cameras are fitted on the acrylic tank to film the pipe conveying fluid movements. Fig. 19 shows a 3D representation of the structure holding the cameras and Fig. 20 presents an exploded view of the layout. To install the cameras on the tank, use the following instructions:

- Clamp the bottom 3D printed part on the acrylic tank bottom edge with the T-slot nuts and the screws.
- Fit the top 3D printed part on the acrylic tank walls.

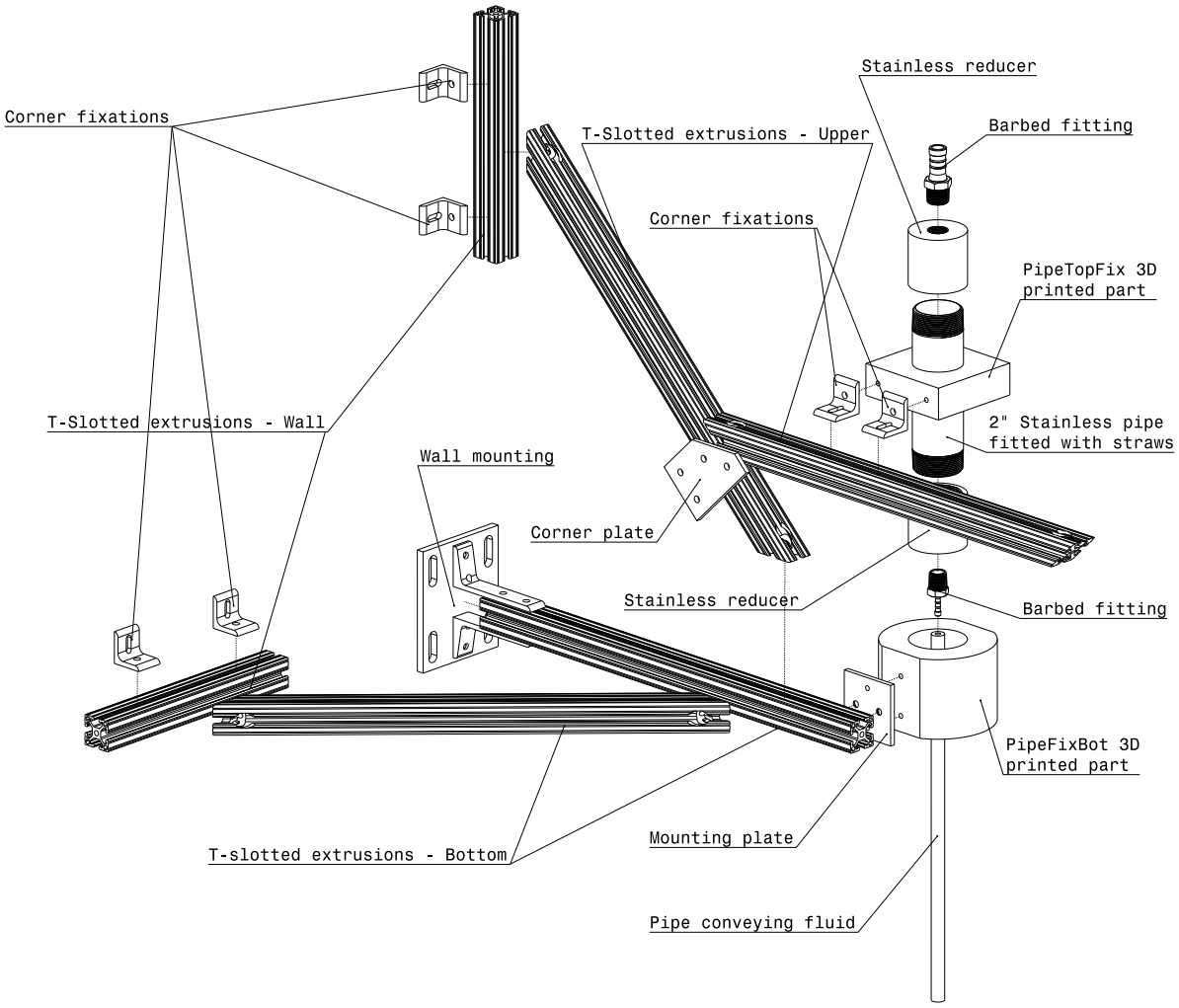

Fig. 13. Exploded view representing the structure supporting the flow-straightener and the pipe conveying fluid clamping.

- Fit the T-slotted extrusion in the holes of the two 3D printed parts and fix it with the corner fixations.
- Fix the corner bracket on the T-slotted extrusion.
- Fix the camera on the corner bracket.
- Adjust the position of the camera by adjusting the height of the bracket and the position of the 3D printed parts on the tank wall.

5.9. Mould assembly

The mould assembly instruction will be presented in the operation section where the use of the mould to cast rubber silicone pipes is described. Indeed, the mould has to be assembled everytime a new pipe is moulded.

6. Operation instructions

6.1. Pipe casting

This section presents the casting process of the pipe conveying fluid. We decided to cast our own pipes to avoid commercial pipes defects.

A room temperature vulcanizing (RTV) rubber-silicon (OOMOO30, Smooth On) was selected to manufacture the pipes. The choice of the rubber-silicon is important to obtain the desired properties for the pipe. It is also important to make sure that the working time is long enough for the moulding process. One of the tricky point is to obtain a pipe rigid enough with a silicon that

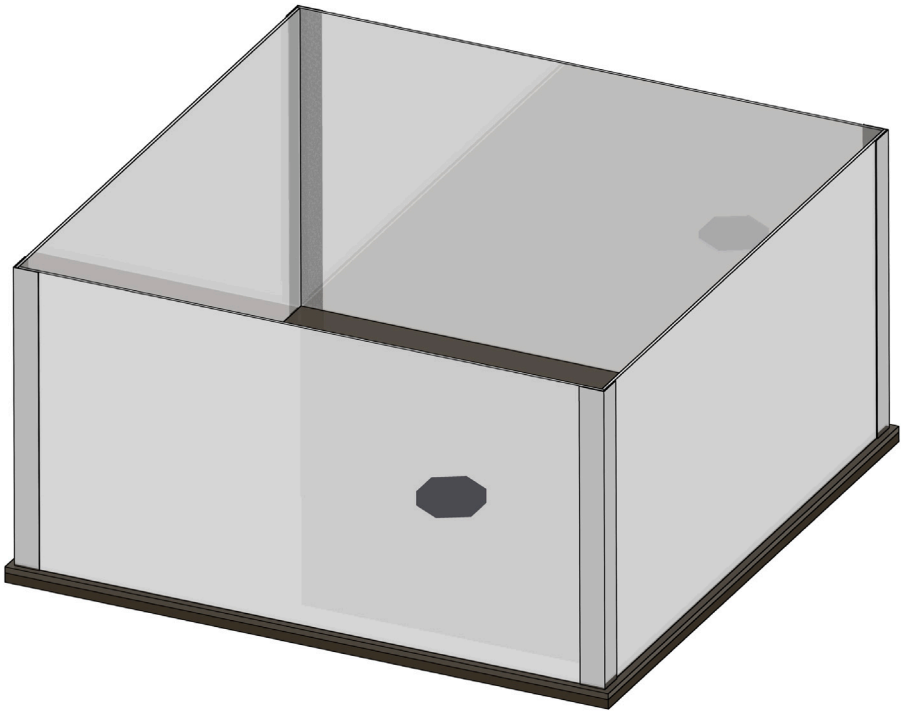

Fig. 14. 3D representation of the acrylic tank.

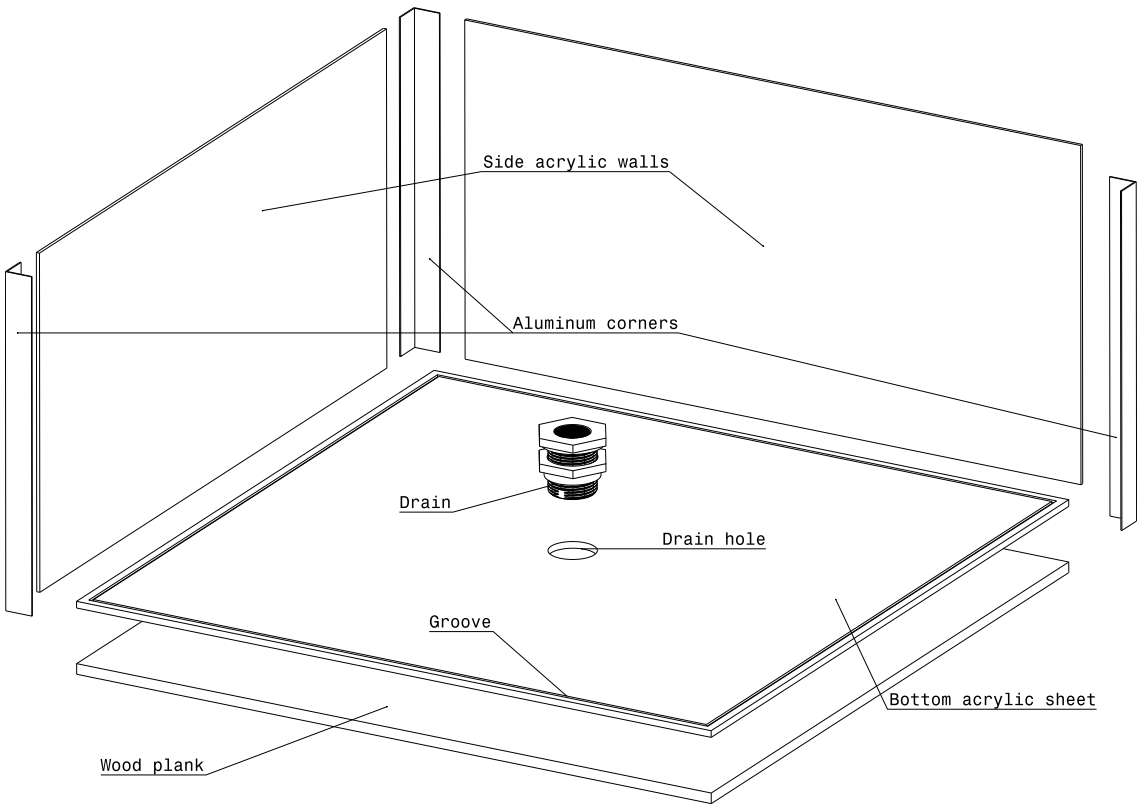

Fig. 15. Exploded view representing the assembly of the acrylic tank.

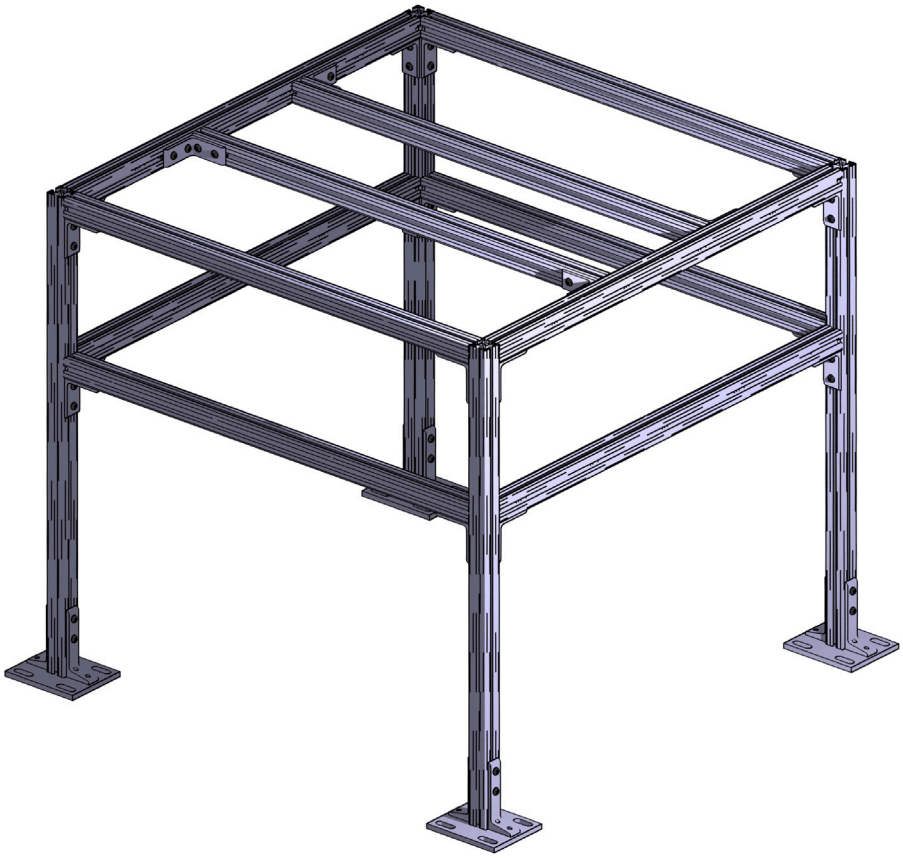

Fig. 16. 3D representation of the acrylic tank supporting structure.

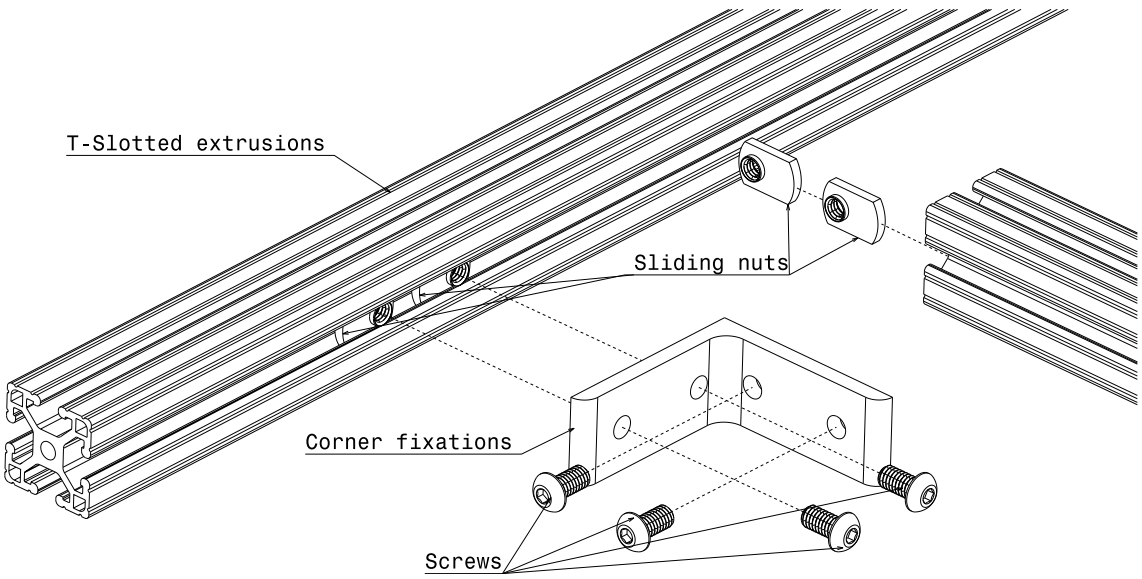

Fig. 17. Exploded view representing the assembly of two aluminium extrusions with a corner.

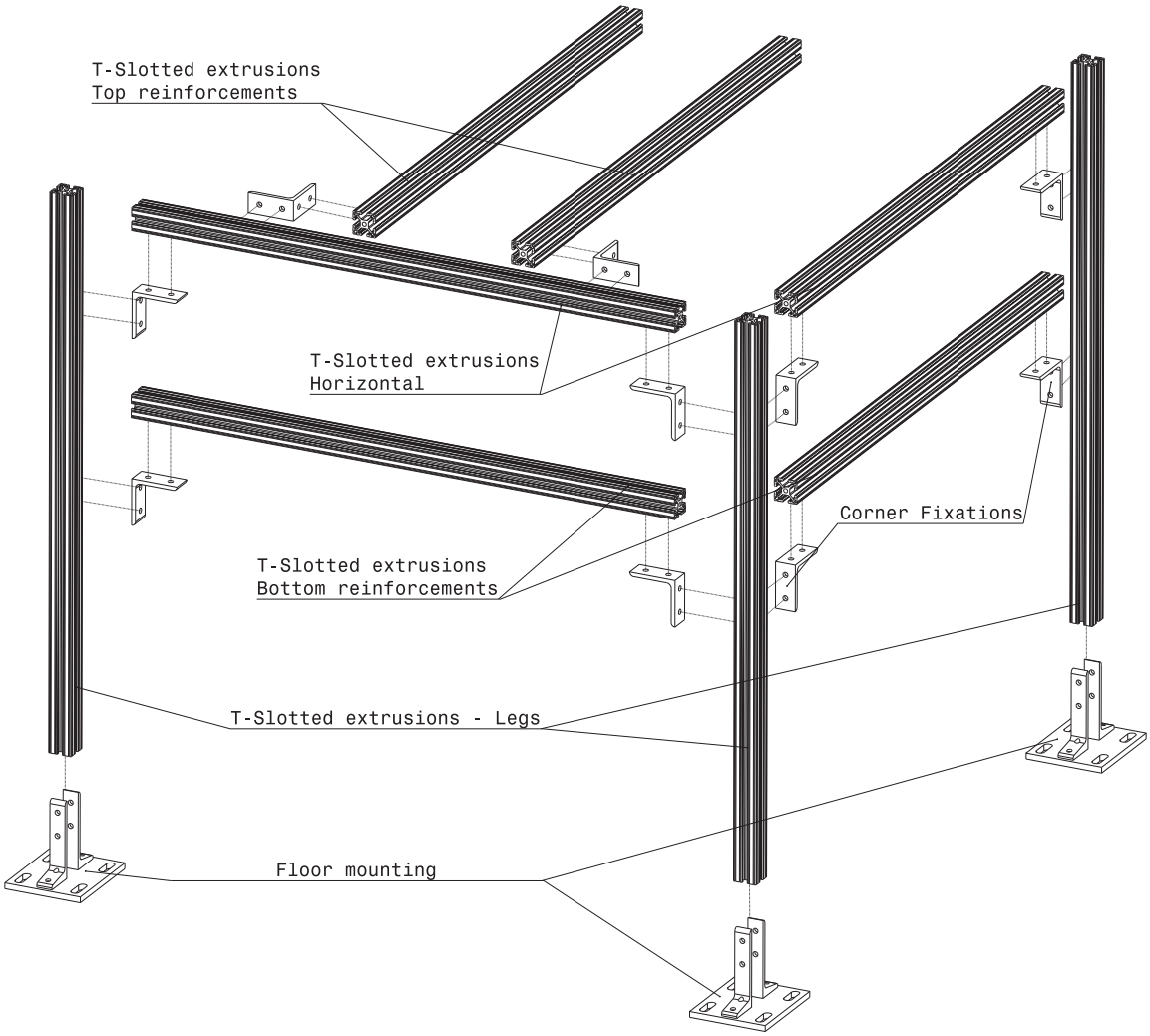

Fig. 18. Exploded view representing the assembly of the acrylic tank support.

is fluid enough. Rubber silicons with a low viscosity are easier to mould into a pipe. In order to obtain more rigid pipe, a rubber silicons with a larger viscosity should be used. However, it will be hard to inject high viscosity rubber silicon in the mould and it could produce bubbles or other defects in the pipe. The chosen rubber-silicon has lavanda colour so we mix black pigments with the rubber-silicone to blacken the pipe to increase the contrast with the white walls and facilitate image treatment.

Fig. 21 shows a 3D representation of the mould and Fig. 22 presents an exploded view of the parts composing the mould.

The detailed procedure to cast a pipe is as follows:

- Perfectly clean all the parts of the mould and spray them with release agent (Universal Mould Release, Smooth On) to facilitate the removal of the pipe from the mould after cure.
- Close the two external aluminium parts of the mould together and adjust their positions by using the dowel pins. Then put the two 3D printed parts on each side of the mould and tighten at the same time the two aluminium parts and the two 3D printed parts with the screws and the threaded rods.
- Position the mould vertically on a pierced wood plank.
- Mix the two components of the rubber-silicon in a large cup according to the supplier instructions. The black pigments are added at this step at a maximum of 3% of the mass of the mix. After a thorough mixing of the two components, the cup is placed in a vacuum chamber for a few minutes to remove air bubbles. Remove the cup from the chamber when no more bubbles are visible.
- Suck the rubber-silicon with a syringe and pour it into the mould from the bottom hole until the mix is spilling out from the top hole. Then, insert the centring rod and block the bottom hole of the mould once the rod is in place.

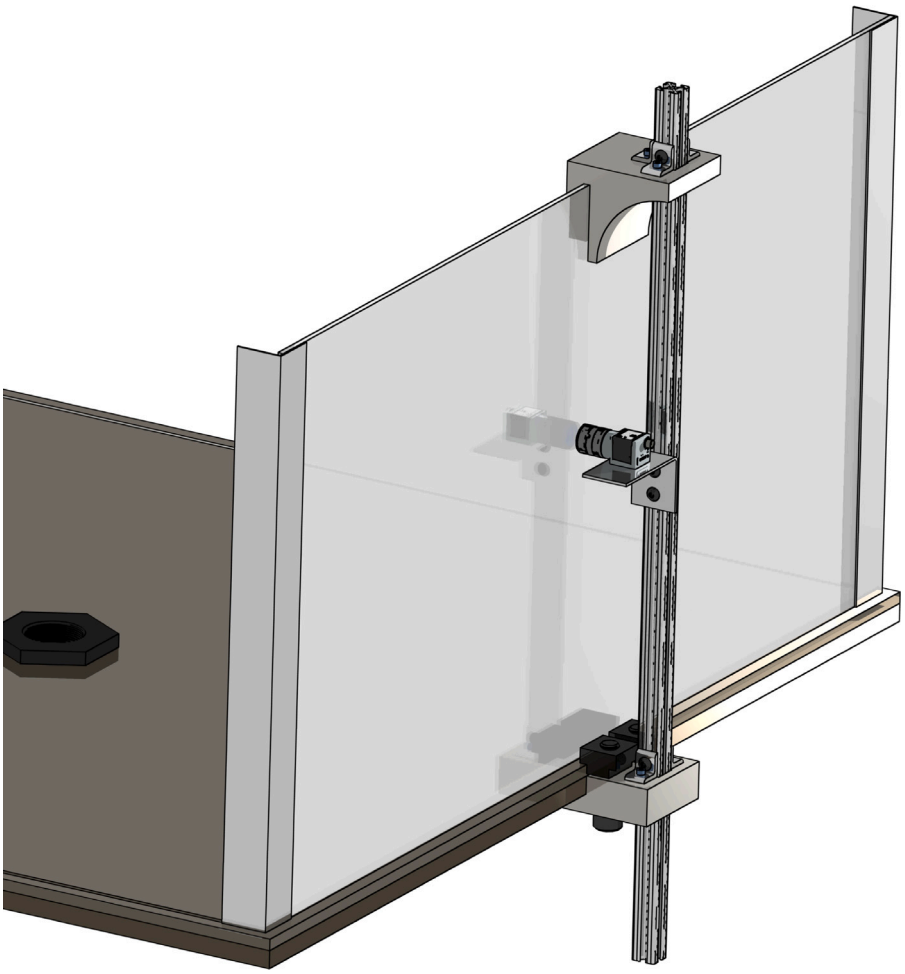

Fig. 19. 3D representation of the structure supporting the cameras.

- After the twelves hour cure time, unmould the pipe by removing the two PLA parts and then the two aluminium parts. The easiest way to remove the centring rods is with a high pressure air gun. Put the tip of the gun between the centring rod and the rubber silicone, inject the air, and then pull the pipe from the rod while continuing to inject the air.
- Cut the pipe to the desired length.

6.2. Water filling

Connect a flexible hose to a water tap and put this flexible pipe in the acrylic water tank which will then drain itself in the main tank.

6.3. Changing the pipe

Follow the subsequent instruction to change the pipe in the setup. Unscrew the screws from the mounting plates used to fix the PipeFixBot 3D printed part. Remove PipeFixBot form the structure holding the pipe conveying fluid. Remove the barbed fitting with the pipe from the bottom stainless reducer. Fit the new barbed fitting with the new pipe with threat sealant tape. Put back in place the PipeFixBot 3D printed part to hold the bottom stainless reducer.

6.4. Water drainage

To empty the water from the system, the operator shall first disconnect the output from the pump and connect it to a long flexible hose. Then put the flexible hose in a sink and activate the pump at low flowrate to empty the main tank in the sink. When the pump starts pumping air, stop immediately to avoid damaging the motor. Afterwards, close the output of the main tank, disconnect it from

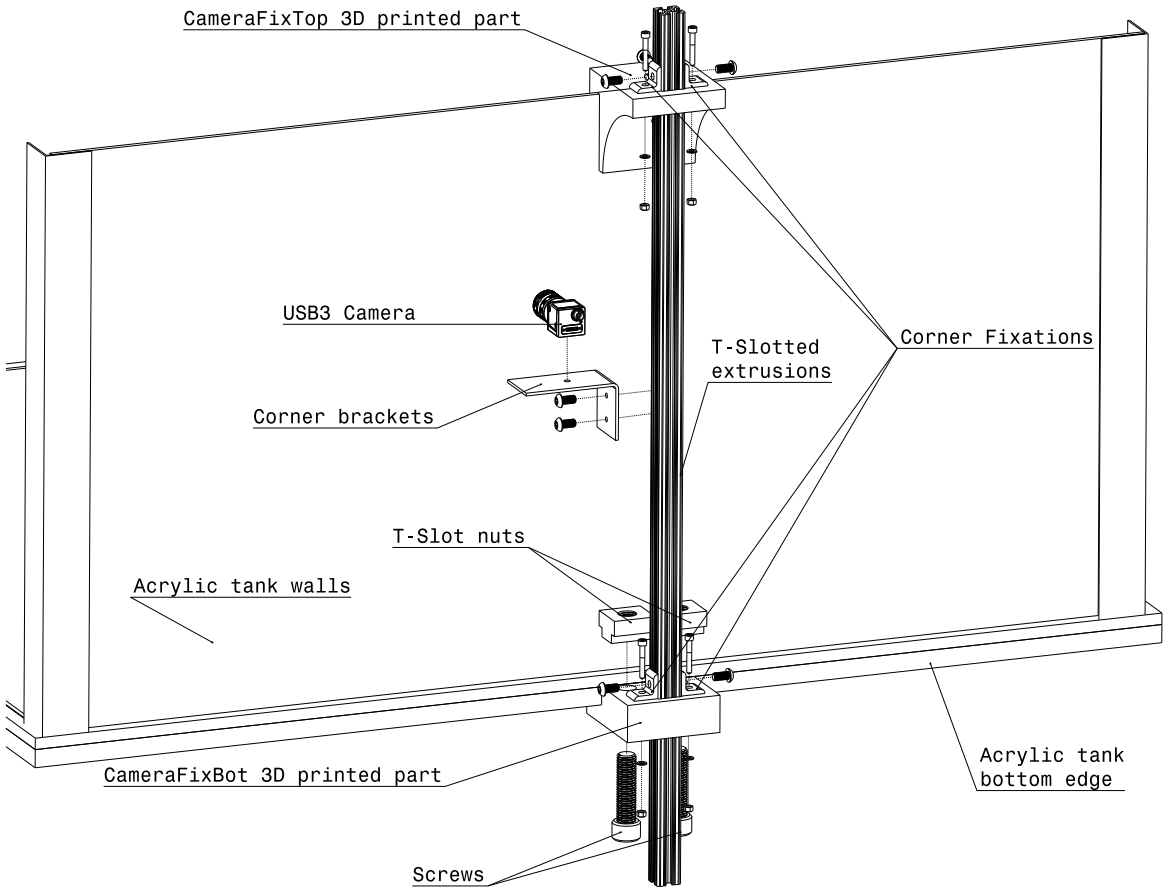

Fig. 20. Exploded view representing the structure supporting the cameras.

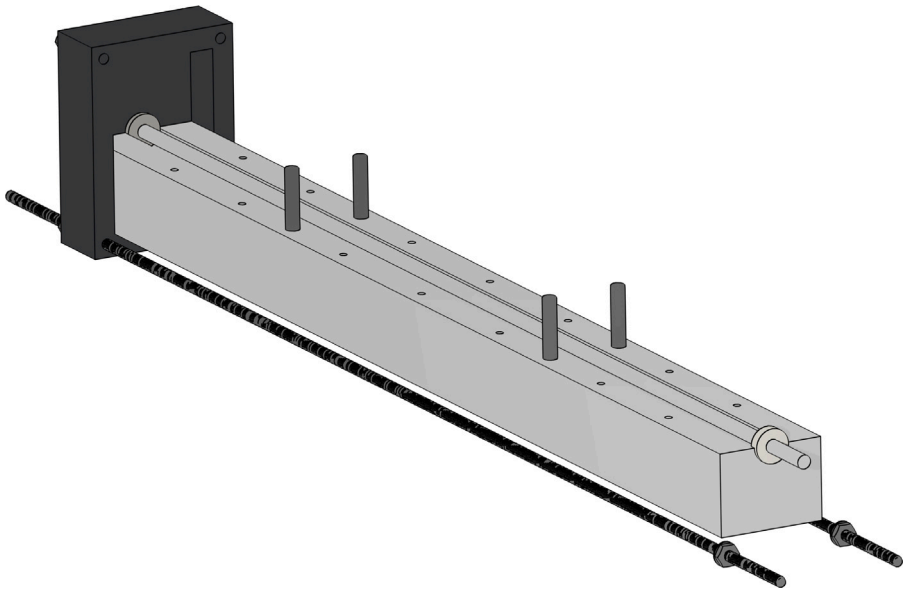

Fig. 21. 3D representation of the mould.

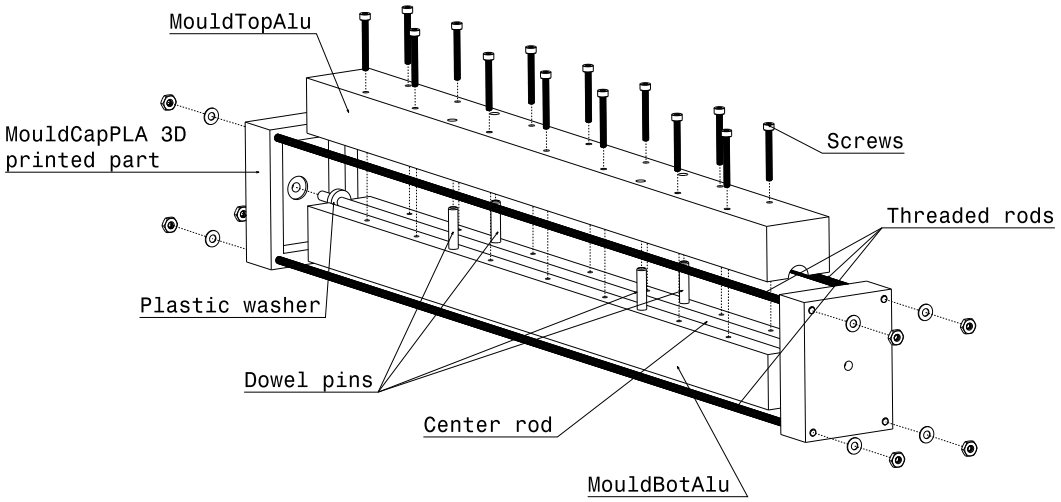

Fig. 22. Exploded view representing the mould.

the pump and carry it to the sink to remove the remaining water. The water level should be low enough to allow the main tank transport.

6.5. Data acquisition system

The pipe is light and very flexible, therefore it is almost impossible to put traditional sensors like strain gauges, pressure sensors or accelerometers on it without altering its dynamics. We therefore use contactless measurements. Most of the literature work use laser distance measuring sensors or points tracking system to track the pipe [9,12,13]. In this project, we want to access data on the whole length of the pipe without limiting ourselves to planar movements. In some configurations, the pipe movement is three-dimensional and it does not make sense to constrain the pipe to a two dimensional movement. We therefore use two high speed cameras to film the pipe from two perpendicular sides.

6.5.1. The cameras

Here we explain how to use the cameras to track the pipe shape in three dimensions.

To synchronize the two cameras, we use a 0–10 V square signal generated with a National Instrument NI9401 card to trigger the acquisition of the two cameras and of the flowmeter to be sure that each camera records a frame simultaneously and that we record the corresponding flowrate. It is important to verify with the cameras software that no images are lost during acquisition to make sure that both cameras stay synchronized.

Image treatment To extract the position of the pipe from the images, we use the contrast between the pipe and the background since the pipe is a dark grey while the background and the liner are plain white. We follow the subsequent procedure to treat the image:

- We convert the image in grey scale using the OpenCV library in Python.
- We convert the image to a binary image which is basically an array where each pixel is either 1 or 0 depending if it is considered black or white. We use the threshold function from OpenCV, depending on the situation and the lighting we use a hard threshold value for the whole image or an adaptive threshold. The values of the thresholds are determined by trial and errors.
- We remove islands of pixel in the image i.e. each detached group of pixel containing a low number of pixels (white or black) is removed to have a better image. This function removes black points corresponding to water splashes and white points on the pipe corresponding to the light reflection.

Once the images are treated as explained above, we proceed to extract the position of the pipe.

Camera calibration The two cameras are fixed on the two sides of the translucent tank and the sensing planes are perfectly parallel to the central plane of the tank. It is therefore not necessary to correct the tangential error. Also, after looking thoroughly at the images, we discovered that the radial distortion is very subtle and we decided to ignore it in the current study. We only have to calibrate the camera to get the origin point of the pipe on the vertical axis, the origin point on the horizontal axis and the scale linking the length in pixels on the image to the length in millimetre on the physical system.

Firstly, to determine the scale of the camera, we printed a black square on a rigid plate and placed it on the planes parallel to each camera at the rest position of the pipe. Knowing the actual size of the square, we find the size in mm of a pixel with the following formula: scale (mm/pixel) $= \frac{\text{square width (mm)}}{\text{square width (pixels)}}$.

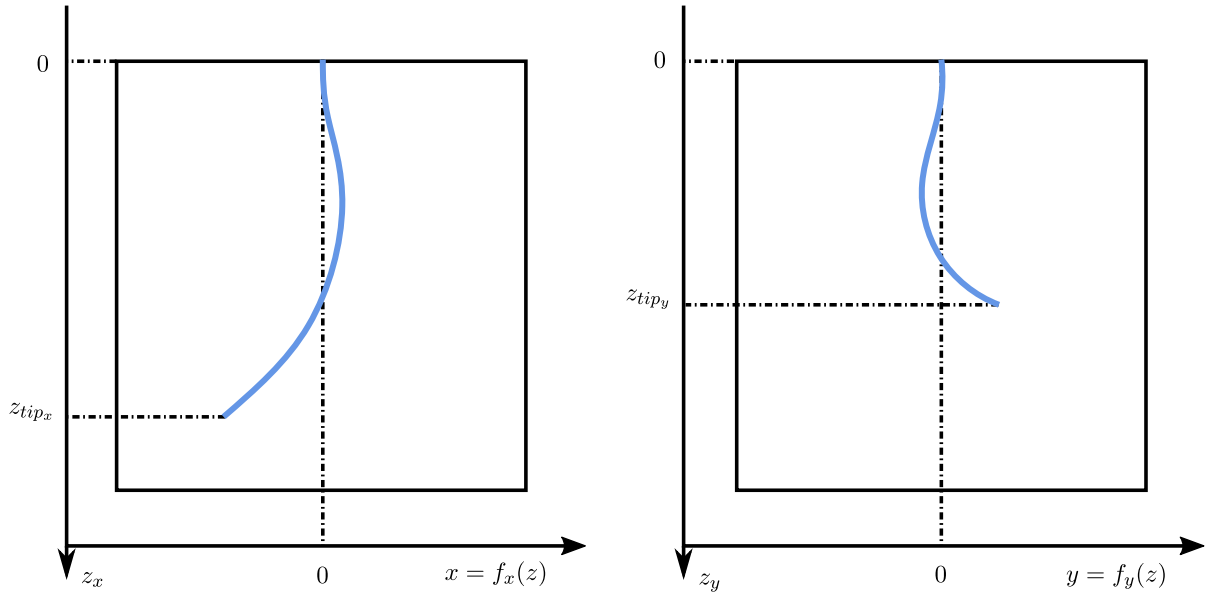

Fig. 23. First step of parallax treatment: Creation of lists of points for both frontal and side images.

Then, to find the origin of the coordinate system, we take a picture of the pipe at rest with no water. We compute the position of the middle line of the pipe which is the origin on the horizontal axis. Then, we find the coordinates of the tip of the pipe on the photo and knowing the length of the pipe, we find the coordinates of the top of the pipe which is the vertical origin point.

For every image in the video, we then have to subtract the coordinates of the origin on the vertical and horizontal axes and multiply by the scale to get the coordinates in mm in the pipe coordinates system.

Extraction of the data from the video Once the images are treated and calibrated, we determine the (x, y, z, t) coordinates of the points on the pipe to train or validate the digital twin. Each image corresponds to a certain time t that is computed with the cameras frame rate. From each image, we extract the coordinates (x, z) from the front and (y, z) from the side of each pixel that is considered black i.e. on the pipe. We fit a polynomial function on the (x, z) and (y, z) to find $x = P(z)$ and $y = P(z)$. This polynomial functions goes through the centreline of the pipe with one condition: the tip of the pipe must be its lowest point. If it is not, there would be two values of y and x for one value of z and the polynomial would not work. We decided not to consider this problem as this configuration rarely appears and only at the highest pump speeds. We then store the coefficients values of the polynomial as well as the position of the tip of the pipe on each camera in a text file.

We then correct one last error on these data: the parallax. The pipe, moving in the tank is getting closer or further than the central plane in which the camera scale was computed. The deflection is therefore overestimated when the pipe is closer to the camera or underestimated when the pipe is further from the camera. We treat this problem by using trigonometry as follows.

We start by creating two lists of N points evenly distributed between $z = 0$ and $z = z_{tip}$ for both cameras. We then compute the lists of the associated deflection x and y with the polynomial functions determined previously. The points with the same index in the lists do not have the same z coordinates because z_{tip} might be higher for one of the camera if the pipe is closer as illustrated on Fig. 23. However, since the points are evenly distributed and since both lists have the same length, we assume that points with the same index in both lists correspond to the same physical point on the pipe.

Then, we correct the y and x coordinate of each points in the lists. We use the Thales theorem as shown in Fig. 24 to compute the actual coordinates x and y from the coordinates observed by the camera in the central plane. We get the following relationships:

$$\frac{y_a}{y_c} = \frac{D_x}{D_x - x_c}, \tag{1}$$

and:

$$\frac{x_a}{x_c} = \frac{D_y}{D_y + y_c}. \tag{2}$$

By combining the previous equations we obtain the following formula for the corrected deflections y_c and x_c:

$$x_c = \frac{x_a D_x (D_y + y_a)}{D_y D_x + y_a x_a}, \tag{3}$$

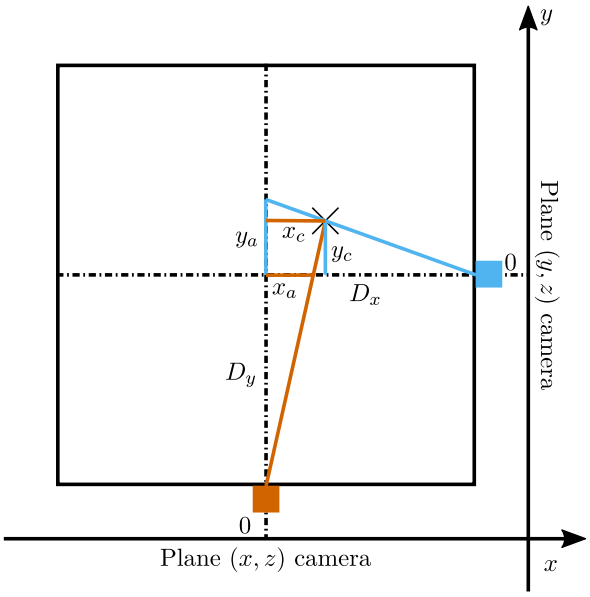

Fig. 24. Second step of parallax treatment: correction of the x and y deflections.

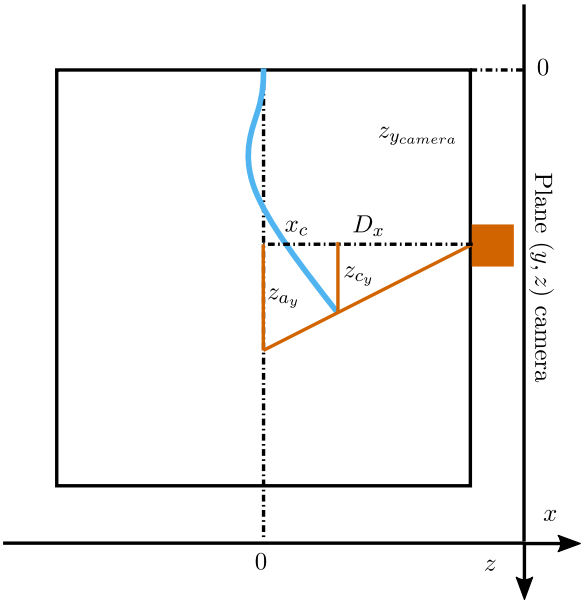

Fig. 25. Third step of parallax treatment: correction of the z height for each points.

and:

$$y_c = \frac{y_a D_y (D_x - x_a)}{D_y D_x + y_a x_a}. \tag{4}$$

With the same Thales theorem, we correct the value of z for each points in the list as shown in Fig. 25. We obtain the following formula for the correction of z for both cameras:

$$z_{x_c} = z_{x_a} \frac{D_y + y_c}{D_y}, \tag{5}$$

and,

$$z_{y_c} = z_{y_a} \frac{D_x - x_c}{D_x}. \tag{6}$$

The corrected value of z on both coordinates should now coincide. The small difference observed is caused by defaults in the image and we merge the two lists of z coordinates in one by taking the average of both.

We then repeat the polynomial fitting step on the z, x and y list after correction to obtain the coefficients of the polynomial valid with corrections.

During image acquisition, some frames are sometimes dropped. This is caused by speed limit of the computer Solid State Drive (SSD), thus letting the computer Random Access Memory (RAM) fill faster than it can be transferred in the SSD memory. This is a big problem when only one camera drops frames, since the frames from both cameras are not synchronized anymore. The software from the camera manufacturer does not allow us to detect reliably when a frame is dropped, so we had to develop our own program to detect it. To do so, we used the fact that the pipe tip height after correction should be the same on both cameras. If the error is too high it means one of two things. Either one of the image is of bad quality, probably because of a splash of water on the glass in front of the camera and the entire pipe cannot be detected or a few frames have been dropped on one camera and the images are not synchronized anymore. We easily identify which case it is by plotting the height error against time. If the error is only spiking for a few frames, then it corresponds to the first case caused by a splash of water. However, when the error is significantly increasing for all the frames, then frames have been dropped on one of the cameras. By looking at these graphics we can easily decide which videos to reshoot.

6.5.2. Flowrate

Here we explain how to use the flowmeter to measure the flow velocity in the pipe conveying fluid.

A magnetic Rosemount 8711 flowmeter with a 3/4" tube and a 8732 transmitter measures the volumic flowrate in the circuit. The 4–20 mA signal is scaled to correspond to a flowrate range from 0 to 50 liters per minute, 50 lpm corresponding to the maximum flowrate that is reached with pipe No. 7. The flow speed is acquired five times per seconds with a National Instrument current acquisition card. The flowrate is computed as the mean of the flow velocity on the whole acquisition period to reduce noise influence. During long operations of the setup, the temperature of the water increases by up to 10 °C. From 20 to 30 °C, the density of water varies from 0.9982 kg/l to 0.9956 kg/l, which represents a 0.26% difference considered negligible in our experiments.

6.5.3. Data storage

The data is stored locally on a local drive. One .csv file with the flowrate recording is saved with two .mp4 videos for each cameras. After the treatment of the videos with Python we keep a .csv file to save the flowrate value and the polynomial coefficients characterizing the shape of the pipe for each time step.

6.5.4. Alternative data acquisition system

We used Labview because we already owned the cards and the software and hence we already had an on the shelf solution for data acquisition. However, a simple Arduino with a current acquisition card and a tension output card would be sufficient to record the flowrate values and trigger the cameras simultaneously.

6.6. Normal operation

To use the setup follow the subsequent steps:

- First adjust the position of both cameras by sliding the 3D printed parts on the acrylic tank walls and by adjusting the height of the corner brackets on the T-slotted extrusions.
- Spray the acrylic walls with water repellent product and put the white liner on top of the acrylic tank to prevent leaks and have a uniform background for the video treatment.
- Make sure that all the valves are open and that there is enough water in the main tank for the pump to run smoothly.
- Turn on the electrical power of the pump and of the flowmeter.
- Turn on the pump at the chosen frequency on the drive.
- Wait for the flowrate to stabilize.
- Start the acquisition of the flowrate of the flowmeter and of the synchronized videos of both cameras.
- When observing the behaviour at low flowrate before instability appears, subject the pipe to a perturbation with a rod thought the white liner. Observe the response of the pipe getting back to its stable rest position.
- Select the new frequency of the pump to change the flowrate and start the acquisition again when the flowrate is stable.

7. Validation and characterization

7.1. Characterization of the pipe

The first step to use this experimental setup is to characterize the pipe. The classic linear partial differential equation of the pipe derived in Ref. [1] models the linear behaviour of the pipe before the destabilization of the motion:

$$\alpha\dot{\eta}'''' + \eta'''' + \left(u^2 - \gamma\left(1-\xi\right)\right)\eta'' + 2\beta^{1/2}u\dot{\eta}' + \gamma\eta' + \ddot{\eta} = 0, \tag{7}$$

where the dimensionless parameters are defined in Table 3.

Table 3
Parameters of the pipe non-dimensional PDE.

Formulation	Signification
$\xi = \frac{z}{L}$	Non-dimensional vertical coordinates
$\eta = \frac{x}{L}$	Non-dimensional deflection of the pipe
$\tau = (\frac{EI}{M+m})^{\frac{1}{2}} \frac{t}{L^2}$	Non-dimensional time
$u = (\frac{M}{EI})^{\frac{1}{2}} LU$	Non-dimensional flowrate
$\beta = \frac{M}{M+m}$	Mass parameter
$\gamma = \frac{(M+m)L^3}{EI} g$	Gravity parameter
$\alpha = (\frac{I}{E(M+m)})^{\frac{1}{2}} \frac{E^*}{L^2}$	Damping parameter
$\dot{} = \frac{\partial}{\partial t}$	Time derivative
$' = \frac{\partial}{\partial z}$	Space derivative

We can identify the different terms of the equation as follows:

- $\alpha\dot{\eta}''''$ is the visco-elastic damping term;
- η'''' is the flexural rigidity term;
- $u^2\eta''$ is the centrifugal force term;
- $-\gamma(1-\xi)\eta'' + \gamma\eta'$ are the term from the influence of gravity;
- $2\beta^{1/2}u\dot{\eta}'$ is the Coriolis force term;
- $\ddot{\eta}$ is the inertial term.

To solve this PDE, we used the Galerkin method as detailed in Ref. [1]. The idea is to write an approximation of the solution as a summation of cantilevered beam eigenfunctions (ϕ_i) with time functions (q_i) as follows:

$$\eta(\xi,\tau) = \sum_{i=1}^{N} \phi_i(\xi) q_i(\tau). \tag{8}$$

The ϕ_i functions are well known and take the following shape:

$$\phi_i(\xi) = cosh(\lambda_i\xi) - cos(\lambda_i\xi) - \sigma_i(sinh(\lambda_i\xi) - sin(\lambda_i\xi)), \tag{9}$$

with λ_i, the cantilevered beam eigenfrequencies satisfying the following:

$$cos(\lambda_i)cosh(\lambda_i) + 1 = 0, \tag{10}$$

and with:

$$\sigma_i = \frac{sinh(\lambda_i) - sin(\lambda_i)}{cosh(\lambda_i) + cos(\lambda_i)}. \tag{11}$$

We inject the series solution of Eq. (8) into Eq. (7), multiply it by $j = 1, 2, \ldots, N$ and integrate the resulting N equations between 0 and 1 on the ξ domain. We obtain the following equations for every $j = 1, 2, \ldots, N$:

$$\begin{aligned}\sum_{i=1}^{N} \Bigg\{ & \alpha \int_0^1 \phi_i(\xi)'''' \phi_j(\xi) \dot{q}_i(\tau) d\xi + \int_0^1 \phi_i(\xi)'''' \phi_j(\xi) q_i(\tau) d\xi \\ & + \left(u^2 - \gamma(1-\xi)\right) \int_0^1 \phi_i(\xi)'' \phi_j(\xi) q_i(\tau) d\xi + 2\beta^{1/2} u \int_0^1 \phi_i(\xi)' \phi_j(\xi) \dot{q}_i(\tau) d\xi \\ & + \gamma \int_0^1 \phi_i(\xi)' \phi_j(\xi) q_i(\tau) d\xi + \int_0^1 \phi_i(\xi) \phi_j(\xi) \ddot{q}_i(\tau) d\xi \Bigg\} = 0.\end{aligned} \tag{12}$$

From the cantilevered beam equation, we obtain:

$$\phi_i(\xi)'''' = \lambda_i^4 \phi_i(\xi). \tag{13}$$

We also use the fact that the cantilevered beam eigenfunctions ϕ are orthonormal meaning:

$$\int_0^1 \phi_i(\xi)\phi_j(\xi) d\xi = \begin{cases} 0 & \text{if } i \neq j \\ 1 & \text{if } i = j \end{cases}. \tag{14}$$

Table 4
Formula for the integral terms of the PDE.

	Case $i = j$	Case $i \neq j$
b_{ij}	2	$\frac{4}{(\frac{\lambda_i}{\lambda_j})^2+(-1)^{i+j}}$
c_{ij}	$\lambda_i\sigma_i(2-\lambda_i\sigma_i)$	$\frac{4(\lambda_i\sigma_i-\lambda_j\sigma_j)}{(-1)^{i+j}-(\frac{\lambda_i}{\lambda_j})^2}$
d_{ij}	$\frac{1}{2}c_{ii}$	$\frac{4(\lambda_i\sigma_i-\lambda_j\sigma_j+2)}{1-(\frac{\lambda_i}{\lambda_j})^4}(-1)^{i+j} - \frac{3+(\frac{\lambda_i}{\lambda_j})^4}{1-(\frac{\lambda_i}{\lambda_j})^4}b_{ij}$

We therefore obtain the following equation:

$$\sum_{i=1}^{N}\left\{\delta_{ij}\ddot{q}_i + \left[\alpha\lambda_i^4\delta_{ij} + 2\beta^{1/2}u\int_0^1 \phi_j\phi_i'\mathrm{d}\xi\right]\dot{q}_i + \left[\lambda_i^4\delta_{ij} + \left(u^2-\gamma\right)\int_0^1 \phi_j\phi_i''\mathrm{d}\xi + \gamma\int_0^1 \phi_j\phi_i'\mathrm{d}\xi + \gamma\int_0^1 \phi_j\xi\phi_i''\mathrm{d}\xi\right]q_i\right\} = 0, \quad j = 1,2,\ldots,N. \tag{15}$$

With the boundary conditions of the cantilevered pipe, one can obtain a formula for the following terms which are presented in Table 4:

$$\int_0^1 \phi_i(\xi)\phi_j(\xi)'d\xi = b_{ij}, \tag{16}$$

$$\int_0^1 \phi_i(\xi)\phi_j(\xi)''d\xi = c_{ij}, \tag{17}$$

$$\int_0^1 \phi_i(\xi)\phi_j(\xi)''\xi d\xi = d_{ij}. \tag{18}$$

We therefore obtain the N following equations for $1 \leq j \leq N$:

$$\sum_{i=1}^{N}\left\{\delta_{ij}\ddot{q}_i + \left[\alpha\lambda_i^4\delta_{ij} + 2\beta^{1/2}ub_{ij}\right]\dot{q}_i + \left[\lambda_i^4\delta_i j + (u^2-\gamma)c_{ij} + \gamma b_{ij} + \gamma d_{ij}\right]q_i\right\} = 0. \tag{19}$$

This equation can be written as a $(N \times N)$ matrix system:

$$\ddot{\boldsymbol{q}} + \left[\boldsymbol{F} + 2\beta^{1/2}u\boldsymbol{B}\right]\dot{\boldsymbol{q}} + \left[\boldsymbol{\Delta} + \gamma\boldsymbol{B} + (u^2-\gamma)\boldsymbol{C} + \gamma\boldsymbol{D}\right]\boldsymbol{q} = \boldsymbol{0}, \tag{20}$$

where the $\boldsymbol{B}$, $\boldsymbol{C}$ and $\boldsymbol{D}$ matrices are $(N \times N)$ matrices respectively containing the values of b_{ij}, c_{ij} and d_{ij}. $\boldsymbol{F}$ and $\boldsymbol{\Delta}$ are diagonal matrices with their respective components being $\alpha\lambda_i^4$ and λ_i^4.

We transform this matrix equation to a classic second order differential matricial equation as follows:

$$\boldsymbol{M}\ddot{\boldsymbol{q}} + \boldsymbol{S}\dot{\boldsymbol{q}} + \boldsymbol{K}\boldsymbol{q} = \boldsymbol{0}\,. \tag{21}$$

We then reduce this system to a first order system as follows:

$$\boldsymbol{Q} = \begin{bmatrix}\dot{\boldsymbol{q}}\\ \boldsymbol{q}\end{bmatrix},\ \boldsymbol{U} = \begin{bmatrix}\boldsymbol{M} & \boldsymbol{S}\\ \boldsymbol{0} & \boldsymbol{1}\end{bmatrix} \text{ and } \boldsymbol{V} = \begin{bmatrix}\boldsymbol{0} & \boldsymbol{K}\\ \boldsymbol{-1} & \boldsymbol{0}\end{bmatrix}. \tag{22}$$

And the equation becomes:

$$\boldsymbol{U}\dot{\boldsymbol{Q}} + \boldsymbol{V}\boldsymbol{Q} = \boldsymbol{0}. \tag{23}$$

We suppose $\boldsymbol{Q} = \boldsymbol{A}e^{\lambda\tau}$, and inject this solution into Eq. (23), to get:

$$(\lambda\boldsymbol{U} + \boldsymbol{V})\boldsymbol{A} = \boldsymbol{0} \leftrightarrow \lambda\boldsymbol{A} = (-\boldsymbol{U}^{-1}\boldsymbol{V})\boldsymbol{A}, \tag{24}$$

where λ is an eigenvalue of $-\boldsymbol{U}^{-1}\boldsymbol{V}$ and $\boldsymbol{A}$ is an eigenvector. This system is solved as an eigenvalues problem with built in functions in Python for example.

It is then possible to compute the eigenfrequencies λ and eigenvectors of $\boldsymbol{q}$ for different values of u, β, γ or α. However, if one wants to study the evolution of these eigenfrequencies with the values of one parameter, then it is necessary to track the modes when the input values change. Indeed, the Python function used to compute the eigenvalues and the eigenvectors returns them in random a order. To plot the evolution of an eigenfrequencies, it is necessary to plot them for the same modes. Therefore, we used the Maximum Assurance Criterion (MAC) to order the output of the Python function according to the correct mode [14].

We applied the following method to sort the results with the correct modes for the evolution of the variable parameter P (that can be u, β, γ or α):

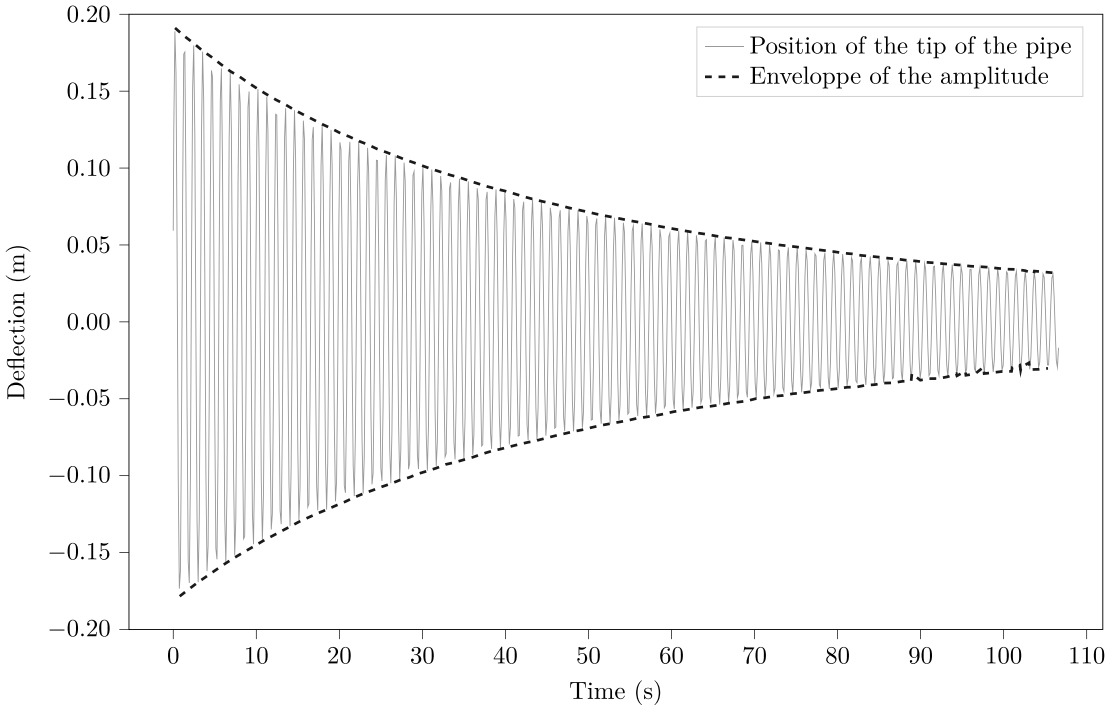

Fig. 26. Position evolution of a pipe of length L = 46 cm, of internal diameter d = 6.35 mm and of external diameter D = 15.875 mm after a perturbation of 0.2 m and without flow.

- At $P = P_{init}$, we sort the modes from smallest to biggest eigenvalue real parts;
- At each $P + \Delta P$, we compute the MAC matrix of every modes from P with every modes from $P + \Delta P$;
- We associate the modes from $P + \Delta P$ with the modes from P with which they have the largest MAC;
- If the MAC is less than 0.9, we go back to the second step with $\Delta P_{new} = \Delta P/2$;

For all the following computations, we used $N = 10$ as the number of beam modes as it is recognized to be enough in the literature. All the codes to solve the linear model and other codes used in the next part of this paper are available at Ref. [15] with the data.

To characterize the pipe, we need to determine the three non-dimensional parameters in Eq. (7). We cannot use the data given by the rubber-silicone manufacturer as they are not accurate and are subjected to changes in different lot numbers. The mass parameter β can be easily determined by measuring and weighting the pipe.

We determined the other two parameters using a method inspired from Paidoussis [16]. We record the pipe in cantilevered configuration with a high speed camera in planar free motion after a planar perturbation of 0.2 m without flow going through the pipe. To observe this movement, we hold the pipe in a perpendicular plane to the camera plane and then release it. An image processing program, presented later, retrieves the amplitude decay and the pipe free motion frequency from the videos. We then use this data to determine the parameters as follows.

Fig. 26 shows the evolution of the position of the tip of a pipe with length $L = 46$ cm, internal diameter $d = 6.35$ mm and external diameter $D = 15.875$ mm along time after perturbation. The grey solid curve shows the position of the tip at each frame and the two black dashed lines follow the decay of the amplitude of the pipe with time. To obtain the evolution of the amplitude, we used the function find_peaks from Scipy in Python to find the peaks of the position of the tip. Fig. 26 confirms that the position of the tip follows a sinusoidal law multiplied by an exponential amplitude term.

We then fitted a linear function to the logarithm of the amplitude from the black dashed lines and performed a FFT on the position of the tip of the pipe in Fig. 27. Fig. 27(a) compares the linear regression results in dashed line and the actual measured amplitude in solid grey line. The overall agreement is good but the logarithmic amplitude is not fully linear which could be explained by the large amplitudes at the beginning of the video. It would be possible to have a better agreement on a smaller range of amplitude at the expense of having to use two coefficients for the full amplitude range. The amplitude logarithmic coefficient is the first term of the linear regression. We performed the operation on three videos and computed the coefficient as an average of the three videos: $\delta = -0.0167$ where δ is the logarithmic amplitude decrement corresponding to the first regression coefficient. Fig. 27(b) shows the result from the FFT of the position of the pipe. This FFT gives us the natural frequency of the pipe without water. As for the logarithmic decay, we filmed three videos and computed the average frequency $f = 0.915$ Hz.

Then we compute the evolution of the non-dimensional fundamental frequency with respect to the γ parameter $Re(\omega_1)(\gamma)$, using the method presented previously to solve the eigenvalues problem for 501 values of γ in the $[0, 500]$ interval and for $u = \beta = 0$. We

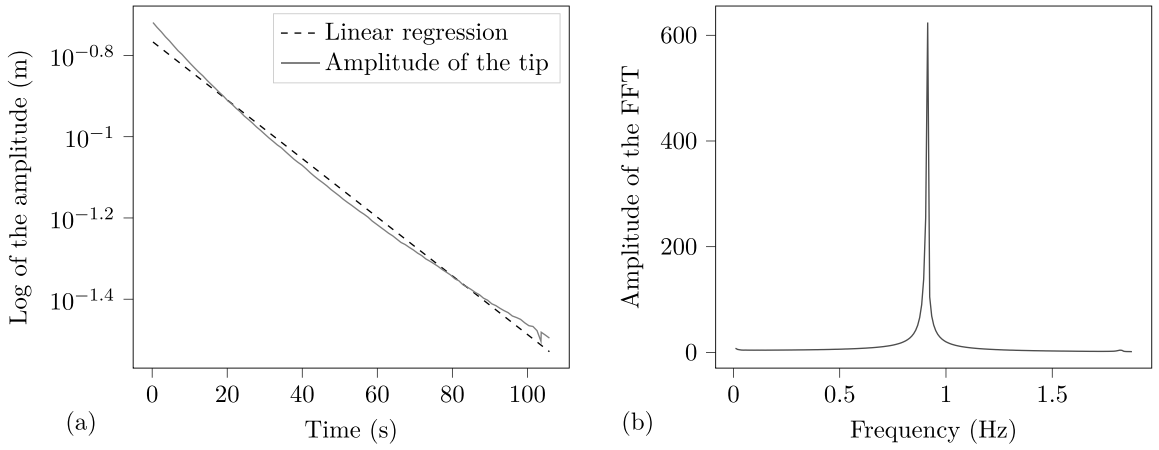

Fig. 27. (a): Comparison of the logarithmic amplitude of the tip and linear regression associated and (b) result of the FFT of the position of the tip.

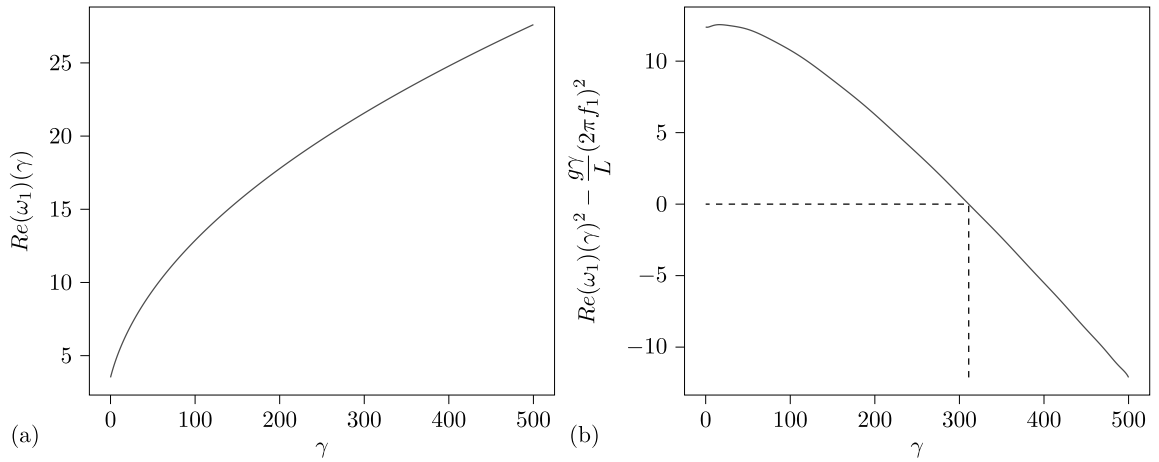

Fig. 28. Determination of the γ parameter: (a) Real part of the first eigenvalue as a function of γ and (b) determination of the value of γ by finding the root of the function constructed with the measured frequency.

notice that $Re(\omega_1)$ is independent of α, so we can generate these points with any values of α. We use $\alpha = 0.02$. We fit $Re(\omega_1)(\gamma)$ with a polynomial function of order 20 to obtain a formulation for γ values in the interval $[0, 500]$. Finally, the relation between the dimensional and the non-dimensional parameters links the measured fundamental frequency of the pipe and the non-dimensional fundamental frequency as follows:

$$\tau = \left(\frac{EI}{M+m}\right)^{\frac{1}{2}} \frac{t}{L^2}, \tag{25}$$

and

$$\gamma = \frac{(M+m)L^3}{EI} g. \tag{26}$$

We rewrite Eq. (25) as:

$$\frac{1}{Re(\omega_1)} = \left(\frac{EI}{M+m}\right)^{\frac{1}{2}} \frac{1}{2\pi f_1 L^2}, \tag{27}$$

where f_1 is the measured fundamental frequency of the pipe without water.

We then combine Eq. (26) with (27) to get the following relation:

$$\frac{\gamma}{Re(\omega_1)^2} = \frac{g}{4\pi^2 f_1^2 L}. \tag{28}$$

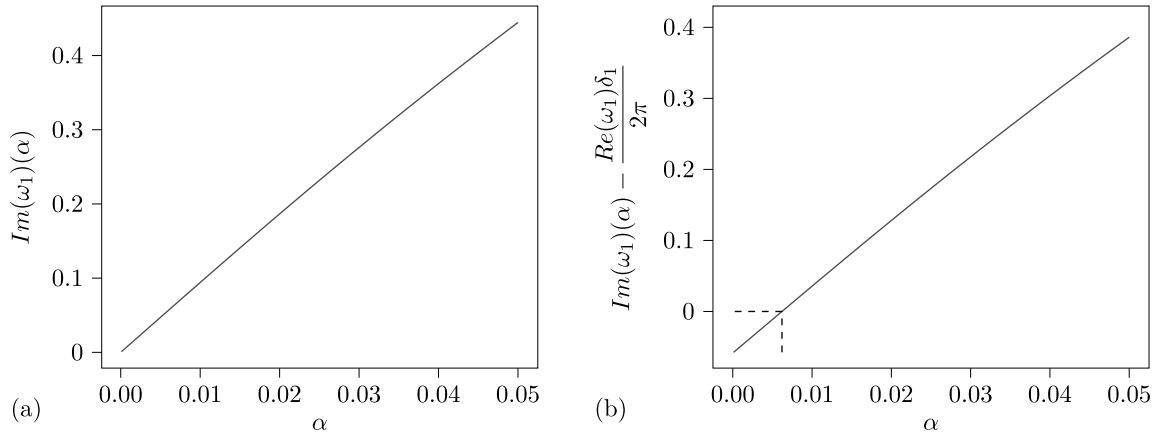

Fig. 29. Determination of the damping parameter α: (a) Imaginary part of the first eigenvalue as a function of α and (b) determination of the value of α by finding the root of the function constructed with the measured frequency.

With the polynomial fit giving $Re(\omega_1)(\gamma) = P(\gamma)$, we can write the following equation:

$$\frac{\gamma}{P(\gamma)^2} - \frac{g}{4\pi^2 f_1^2 L} = 0. \tag{29}$$

A Newton solver finds the root of Eq. (29) to obtain the correct value of γ. We then get the value of E, the pipe Young modulus, using Eq. (26). Fig. 28 shows how to determine the γ parameter of the pipe from the measurement of the pipe natural frequency f_1. Fig. 28(a) corresponds to the polynomial fitting the evolution of the real part of the eigenfrequency with respect to gamma. Fig. 28(b) shows the solution of the Newton solver to find the value of γ from Eq. (29).

We follow a similar method to find the damping parameter α. We use 501 values of α in the $[0, 0.05]$ interval to compute the evolution of the imaginary part of the non-dimensional fundamental frequency with respect to the α parameter $Im(\omega_1)(\gamma)$ and then we fit an order 20 polynomial to get a relation.

We then use the following relation:

$$\delta_1 = \frac{2\pi Im(\omega_1)}{Re(\omega_1)}, \tag{30}$$

where δ_1 is the logarithmic amplitude decrement of the pipe and with the value of $Re(\omega_1)$ from the previous step.

We have to find the root of the following equation to find the value of α:

$$\delta - \frac{2\pi P(\alpha)}{Re(\omega_1)} = 0, \tag{31}$$

where δ is the measured amplitude decay and $Re(\omega_1)$ is known from the step before. This way we determine the value of α and then the value of the damping parameter E^*.

Fig. 29 represents the imaginary part of the pipe first eigenvalue with respect to alpha on the left. On the right the function to determine alpha with the Newton algorithm is shown.

7.2. Validation of the setup

In this section we present results obtained with the experimental setup to demonstrate its ability to study the pipe behaviour.

Fig. 30 shows snapshots of a pipe observed in its flutter plane for different flowrates. These images are taken every 0.02 s and are obtained after treating the images from the cameras.

Fig. 30(a) shows classic first mode flutter which is observed at relatively low flowrate and corresponds to the 2D cycle motion. On the left figure we can observe the first mode of the pipe and a combination of the two first modes on the right figure. Fig. 30(b) shows the shapes at the highest non-dimensional flowrate $u = 30.20$ where the 3D cycle motion is observed. The amplitude is higher than for the previous ones and we observe the third pipe mode. Fig. 30(b) shows unconventional mode shapes as the tip of the pipe goes over the bottom position of the pipe. This figure can be compared to Figure 3.45 of Ref. [1] showing sequences of the limit-cycle motion of a cantilevered pipe conveying fluid.

Fig. 31 represents the trace of the tip of the pipe in the horizontal (x, y) plane for different pipes and flowrates with interesting phenomena. Fig. 31(a) shows the trace for a low flowrate above the critical speed. At this flowrate, the movement of the pipe is planar and stays in the same plane which is at 45° between the two cameras. It is the preferred vibration plane of the pipe which is caused by the imperfections of the pipe itself and of the fixation. This movement type is called the 2D limit cycle motion. When the flowrate increases further as in Fig. 31(b), the movement stays planar but the plane of motion rotates with time. Then, when the flowrate is increased almost to the maximum capability of the system, the pipe motion becomes erratic and completely three

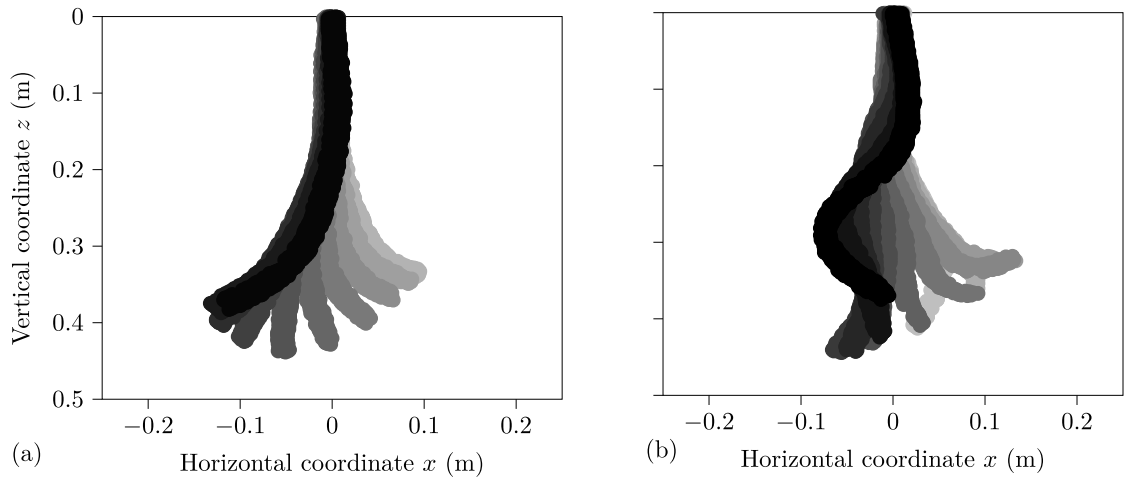

Fig. 30. Snapchots of the pipe with length 46 cm and inner diameter 6.35 mm taken every 0.02 s for different non-dimensional flowrates (a): $u = 21.98$, (b): $u = 30.20$.

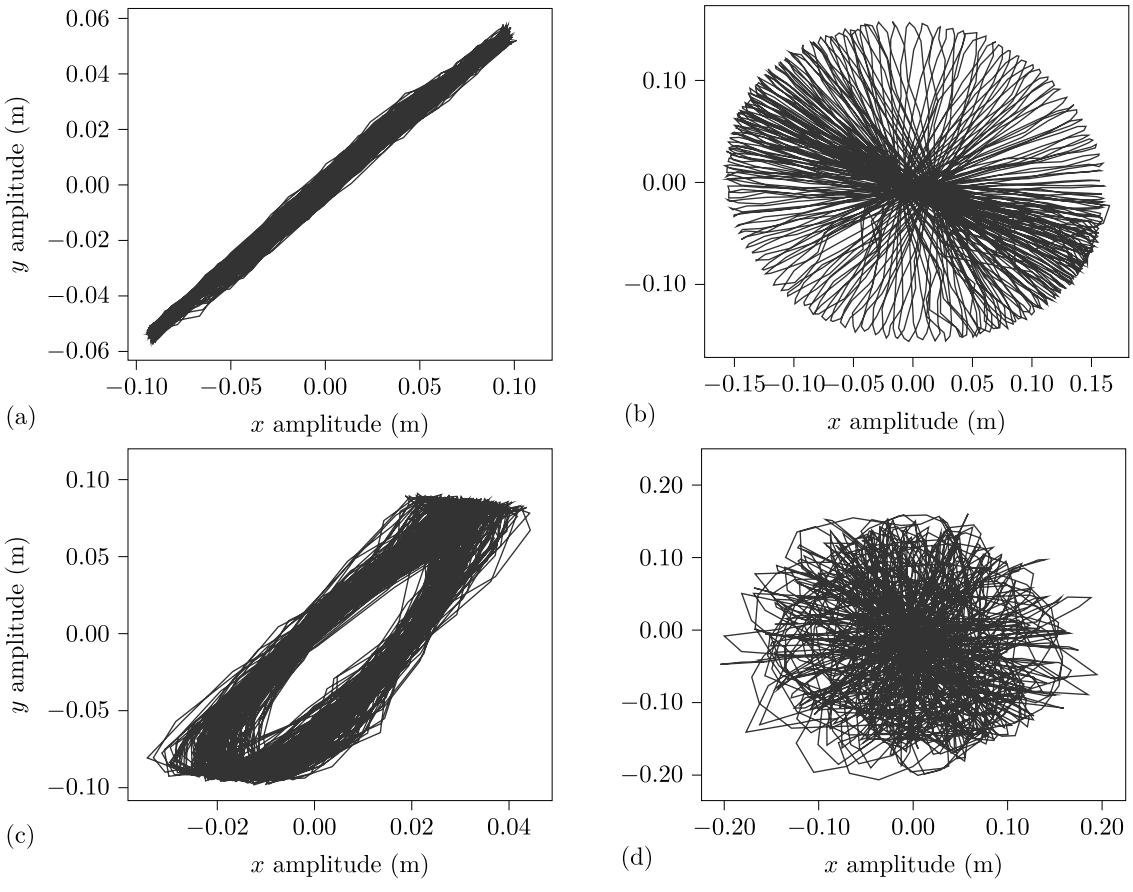

Fig. 31. Trace of the tip of the pipe in the (x, y) plane for different pipes and reduced flowrates: (a) $d = 6.35$ mm, $L = 46$ cm and $u = 17.49$, (b) $d = 6.35$ mm, $L = 46$ cm and $u = 22.70$, (c) $d = 6.35$ mm, $L = 46$ cm and $u = 30.21$ and (d) $d = 9.525$ mm, $L = 46$ cm and $u = 63.95$.

dimensional as shown in Fig. 31(d). In particular conditions, Fig. 31(c) shows a circular three dimensional movement producing an ellipse in a 45° plane. This movement is called the 3D limit cycle motion or the orbital motion. These figures are classic figures that can be compared to Figure 5.49 from Ref. [1] showing typical traces of motion for pipes transitioning from equilibrium to chaos.

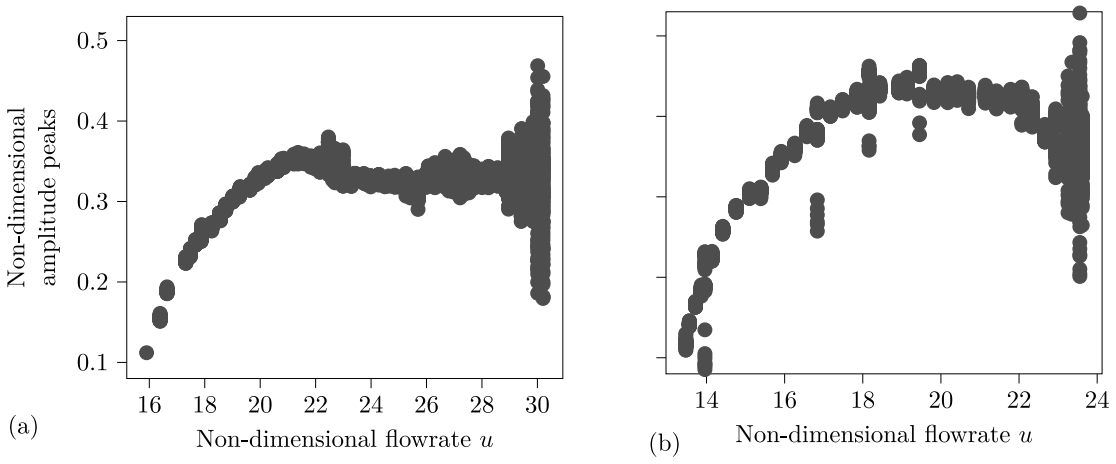

Fig. 32. Peaks amplitude evolution with the non-dimensional flowrate for two pipes of different length: (a) d = 6.35 mm, L = 46 cm and (b) d = 6.35 mm, L = 36 cm.

Lastly, we studied the evolution of the amplitude of the tip of the pipe. We firstly plot the peak amplitude for two different pipes of the same inner diameter 6.35 mm and of length 46 cm and 36 cm in Fig. 32. To obtain this figure, we used a Python function to retrieve the amplitude peaks of the tip of the pipe from the experimental amplitude data from a 30 s long video.

Fig. 32 represents the upper half part of a bifurcation diagram. Indeed, since the motion is three-dimensional, we plot the peaks of the absolute value of the amplitude defined as $\sqrt{(x^2 + y^2)}$. We therefore only have access to the positive part of the amplitude.

At the lowest flowrate, we observe the first bifurcation around $u = 15.9$ and $u = 13.2$ when the pipe loses stability by flutter and the amplitude of the pipe deflection increases. The peaks amplitude then stabilizes when the flowrate increases before reaching the second bifurcation. At the second bifurcation, we observe the period doubling phenomenon as the amplitude peaks have a range of different values for the same flowrate. The pipe from Fig. 32(a) is longer than the pipe from Fig. 32(b) and the bifurcations appear at larger reduced velocity for this first pipe since it is more stable.

These bifurcation diagrams can also be compared to Figure 5.34 and 5.40.a of Ref. [1] which shows the full bifurcation diagram of a cantilevered pipe.

8. Conclusion

In this article, we showed how to build a pipe conveying fluid experimental setup with its instrumentation and data acquisition system. The current experimental setup not only allows us to study the behaviour of the classic cantilevered pipe but can also be easily modified to implement other boundary conditions or pipe features. The measurement system is composed of two high speed cameras and one flowmeter that allows to reconstruct the three dimensional behaviour of the pipe for any flowrate without using disruptive sensors. We conducted experimental campaigns on pipes of different lengths and inner diameters and showed that this setup allows to reproduce classic results from the literature. This setup provides actual experimental data comparable to data available in industrial applications with defects and phenomena that cannot be modelled in a classic simulation. This setup will be a test bench to develop methods for state estimation, parameter identification and test digital twins concepts.

CRediT authorship contribution statement

Morgan Demenois: Conceptualization, Methodology, Software, Validation, Experimental preparation, Writing – original draft. **Hong Yan Miao:** Methodology, Experimental preparation, Project administration, Writing – review & editing. **Frédérick P. Gosselin:** Supervision, Funding acquisition, Project administration, Writing – review & editing.

Declaration of competing interest

The authors declare that they have no known competing financial interests or personal relationships that could have appeared to influence the work reported in this paper.

Acknowledgements

This work was funded by Hydro Quebec, Maya HTT, Innovée and the CRSNG. The author acknowledges the help from the technicians and workers from Polytechnique Montréal, more specifically Bénédict Besner, Fabrice Danet, Philippe Massé, André Francoeur and Albert Gaumond. We are also thankful to Arnaud Divialle, Christian Semler, Barry Turner and Rémi Duquette for their technical and theoretical insight as well as to the members of the LM2 laboratory.

References

[1] M.P. Païdoussis, Fluid-Structure Interactions - Slender Structures and Axial Flow, Vol. 1, 2nd Edition, Elsevier, 2014.
[2] M. Paı, T. Luu, S. Prabhakar, et al., Dynamics of a long tubular cantilever conveying fluid downwards, which then flows upwards around the cantilever as a confined annular flow, J. Fluids Struct. 24 (1) (2008) 111–128.
[3] M. Paı, et al., The canonical problem of the fluid-conveying pipe and radiation of the knowledge gained to other dynamics problems across applied mechanics, J. Sound Vib. 310 (3) (2008) 462–492.
[4] M. Paıdoussis, G. Li, Pipes conveying fluid: A model dynamical problem, J. Fluids Struct. 7 (2) (1993) 137–204.
[5] M. Paidoussis, C. Semler, Non-linear dynamics of a fluid-conveying cantilevered pipe with a small mass attached at the free end, Int. J. Non-Linear Mech. 33 (1) (1998) 15–32.
[6] M. Païdoussis, C. Semler, M. Wadham-Gagnon, S. Saaid, Dynamics of cantilevered pipes conveying fluid. Part 2: dynamics of the system with intermediate spring support, J. Fluids Struct. 23 (4) (2007) 569–587.
[7] O. Doaré, E. de Langre, Effect of Length on the Instability of Hanging Pipes, in: ASME International Mechanical Engineering Congress and Exposition, vol. 5th International Symposium on Fluid Structure Interaction, Aeroelasticity, and Flow Induced Vibration and Noise, 2002, pp. 1223–1232, http://dx.doi.org/10.1115/IMECE2002-39018.
[8] R. Shilling III, Y.K. Lou, An experimental study on the dynamic response of a vertical cantilever pipe conveying fluid, J. Energy Resour. Technol. 102 (3) (1980) 129–135, http://dx.doi.org/10.1115/1.3227862.
[9] K. Yamashita, H. Furuya, H. Yabuno, M. Yoshizawa, Nonplanar vibration of a vertical fluid-conveying pipe (effect of horizontal excitation at the upper end), J. Vib. Acoust. 136 (4) (2014).
[10] C. Semler, Pipe Conveying Fluid: A Paradigm of Nonlinear Dynamics (Ph.D. thesis), McGill University, 1996.
[11] M. Demenois, Design files repository, 2022, http://dx.doi.org/10.17632/xtwrf8859b.3.
[12] M.H. Ghayesh, M.P. Paï¨ doussis, Dynamics of a fluid-conveying cantilevered pipe with intermediate spring support, in: Fluids Engineering Division Summer Meeting, Vol. 54518, 2010, pp. 893–902.
[13] S. Rinaldi, M. Païdoussis, Dynamics of a cantilevered pipe discharging fluid, fitted with a stabilizing end-piece, J. Fluids Struct. 26 (3) (2010) 517–525.
[14] M. Pastor, M. Binda, T. Harčarik, Modal assurance criterion, Procedia Eng. 48 (2012) 543–548.
[15] M. Demenois, Python codes and data used in this project, 2022, URL https://github.com/lm2-poly/PCF_Setup_Article/tree/main/Python_codes.
[16] M. Paidoussis, P. Des Trois Maisons, Free vibration of a heavy, damped, vertical cantilever, J. Appl. Mech. (1971).

Morgan Demenois is a senior analyst in structural engineering at Pratt & Whitney Canada where he works on vibratory analysis and tests of engine parts. He studied aerospace engineering at ISAE-SUPERO and got his master in mechanical engineering at Polytechnique Montréal. During his studies, Morgan worked on the design and construction of small rockets. He also conducted a research project on the use of the Pipe Conveying Fluid experiment as a model experiment to develop digital twins. He is interested in aerospace engineering, vibrations and artificial intelligence applications.

Hong Yan Miao is a research associate at Polytechnique Montreal. She received her Ph.D. degree in 2010 and has over 20 years research experience in mechanical engineering field. She has been collaborated with many industrial partners for research projects, which include design, testing of the equipment and optimization of the manufacturing process. Hong Yan' research interests include finite element simulation and experimental studies of metal forming, surface enhancement, and reducing of the vibration of rotor system, etc.

Frédérick P. Gosselin is a professor of mechanical engineering at Polytechnique Montréal and co-director of the Laboratory for Multiscale Mechanics. He possesses B.Eng and M.Eng degrees in mechanical engineering from McGill University where he had chance to be introduced to research by Prof. Michael P. Païdoussis. He completed his doctoral thesis under the supervision of Prof. Emmanuel de Langre at École Polytechnique in France. He is an expert in fluid–structure interactions and slender structure mechanics. His research interests are broad, with recent contributions inspired by the natural world: soft coral dynamics, spider silk biomimetism, plant cell morphogenesis; as well as applied research: aircraft wing panel forming, 3D printing, and hydroelectric turbine runner vibrations.